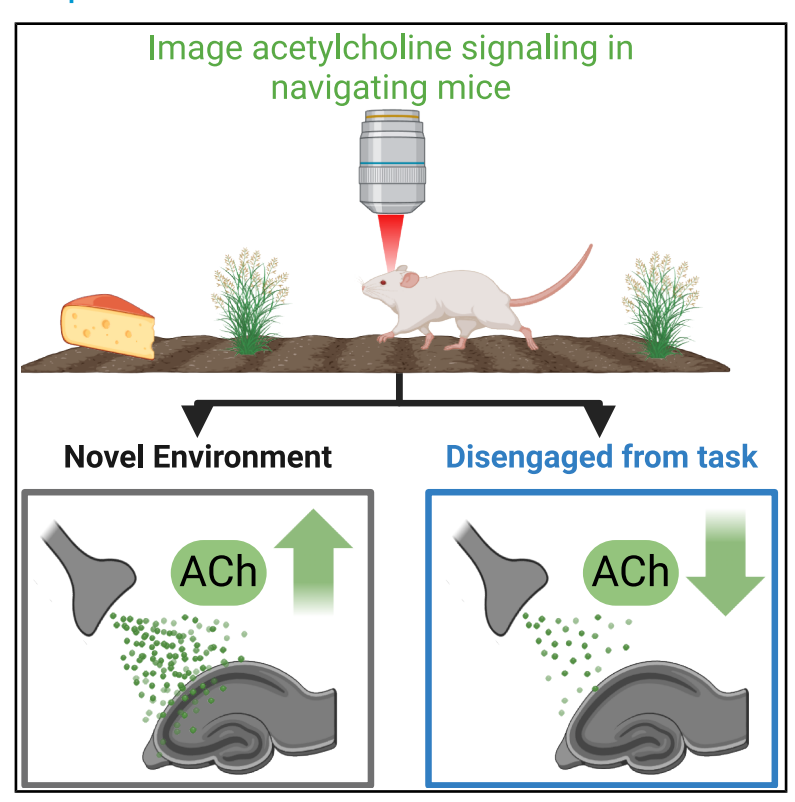
Modulation of speed-dependent acetylcholine release in the hippocampus by spatial task engagement

Graphical abstract



Authors

Feng Xuan, Guochuan Li, Yulong Li, Daniel A. Dombeck

Correspondence

d-dombeck@northwestern.edu

In brief

Xuan et al. measure release of the brain modulation chemical acetylcholine in the mouse hippocampus with micron scale and sub-second resolution. They find increases in release related to heightened attention states and decreases related to task disengagement. Their findings point to a potential mechanism for spatial memory encoding, storage, and recall.

Highlights

- Acetylcholine release changes measured in mouse hippocampus during spatial behavior
- Release was positively correlated to mouse locomotion speed
- Speed-correlated release increased during novel environment exposure
- Speed-correlated release decreased when mice disengaged from the task







Article

Modulation of speed-dependent acetylcholine release in the hippocampus by spatial task engagement

Feng Xuan,¹ Guochuan Li,^{2,3} Yulong Li,^{2,3} and Daniel A. Dombeck^{1,4,*}

SUMMARY

Acetylcholine (ACh) plays important roles in memory encoding and attention in the hippocampus. However, changes in ACh signaling patterns during different neural and behavioral states remain poorly understood. Here, we used a genetically encoded ACh sensor and multi-plane, dual-color two-photon microscopy to establish the ACh signaling patterns in hippocampal CA1 of mice performing spatial behaviors. We observed spatially homogeneous signaling across volumes spanning hundreds of microns, which was positively correlated with locomotion speed. In novel environments, there was an increase in release persisting for dozens of laps while maintaining a positive speed correlation. When mice voluntarily disengaged, the magnitude of the speed-correlated release decreased, and this was accompanied by reduced place cell numbers and less precise place maps. Administration of scopolamine mimicked the effects of voluntary disengagement in terms of behavior and place cell metrics. These findings establish behaviorally correlated ACh signaling patterns in the hippocampus.

INTRODUCTION

Across different brain regions, acetylcholine (ACh) plays important roles in many cognitive processes such as memory encoding and retrieval, arousal states, attention modulation, and locomotion speed encoding. 1-6 In the hippocampus, ACh has long been discussed as a key neuromodulator involved in memory encoding, retrieval, and consolidation.⁷ It was theorized that high ACh concentration (high ACh release) configures the hippocampal circuitry for memory encoding, while low ACh concentration (low ACh release) configures the circuitry for memory consolidation and retrieval.8 Several experiments have provided evidence supporting this model. For example, transferring rats from familiar to novel environments was shown using microdialysis measurements to increase ACh release in the hippocampus over tens of minutes, consistent with a role in memory encoding.9 Consistently, a separate study used immunotoxic lesions of the septo-hippocampal cholinergic neurons to prevent this increased release of ACh and found that this largely prevented place cell remapping in novel environments. 10 However, in the microdialysis study, the increase of ACh release was also accompanied by heightened motor activity. Since ACh release also positively correlates with locomotor activities, 11,12 this poses a challenge to disentangle the contribution of novelty vs. increased motor activity to the elevation of ACh release during such experiences.

In addition to its roles in memory processes, changes in ACh release are thought to be involved in modulating attention, and the muscarinic antagonist scopolamine can induce impairment in attention. 13 For example, recent studies using choline-sensitive microelectrodes² and biosensors¹⁴ demonstrated that phasic acetylcholine release in rodent hippocampus and prefrontal cortex signals successful cue detection, but such release is absent in trials where the cue is missed, suggesting that phasic ACh release in the hippocampus might be involved in processing and attending to relevant sensory information. Further, in humans, muscarinic receptor antagonists like scopolamine impairs memory encoding and immediate recall but spares retrieval of memories encoded prior to drug administration. 15 Moreover, scopolamine also affects spatial navigation abilities of humans in real-world mazes, leading to longer distances traveled to goal locations.¹⁶ However, the spatiotemporal patterns of ACh release in the hippocampus during such spatial behaviors and whether it is modulated by different behavioral and hippocampal network states are poorly understood. Additionally, it is unclear how hippocampal place cell firing patterns change in relation to the changes in spatial navigation abilities induced by scopolamine administration.

To address these gaps in understanding, here we utilized a genetically encoded acetylcholine sensor GRAB-ACh4I,



¹Department of Neurobiology, Northwestern University, Evanston, IL 60208, USA

²State Key Laboratory of Membrane Biology, School of Life Sciences, Peking University, Beijing 100871, China

³Peking-Tsinghua Center for Life Sciences, New Cornerstone Science Laboratory, Academy for Advanced Interdisciplinary Studies, Peking University, Beijing 100871, China

⁴Lead contact

^{*}Correspondence: d-dombeck@northwestern.edu https://doi.org/10.1016/j.celrep.2025.116443



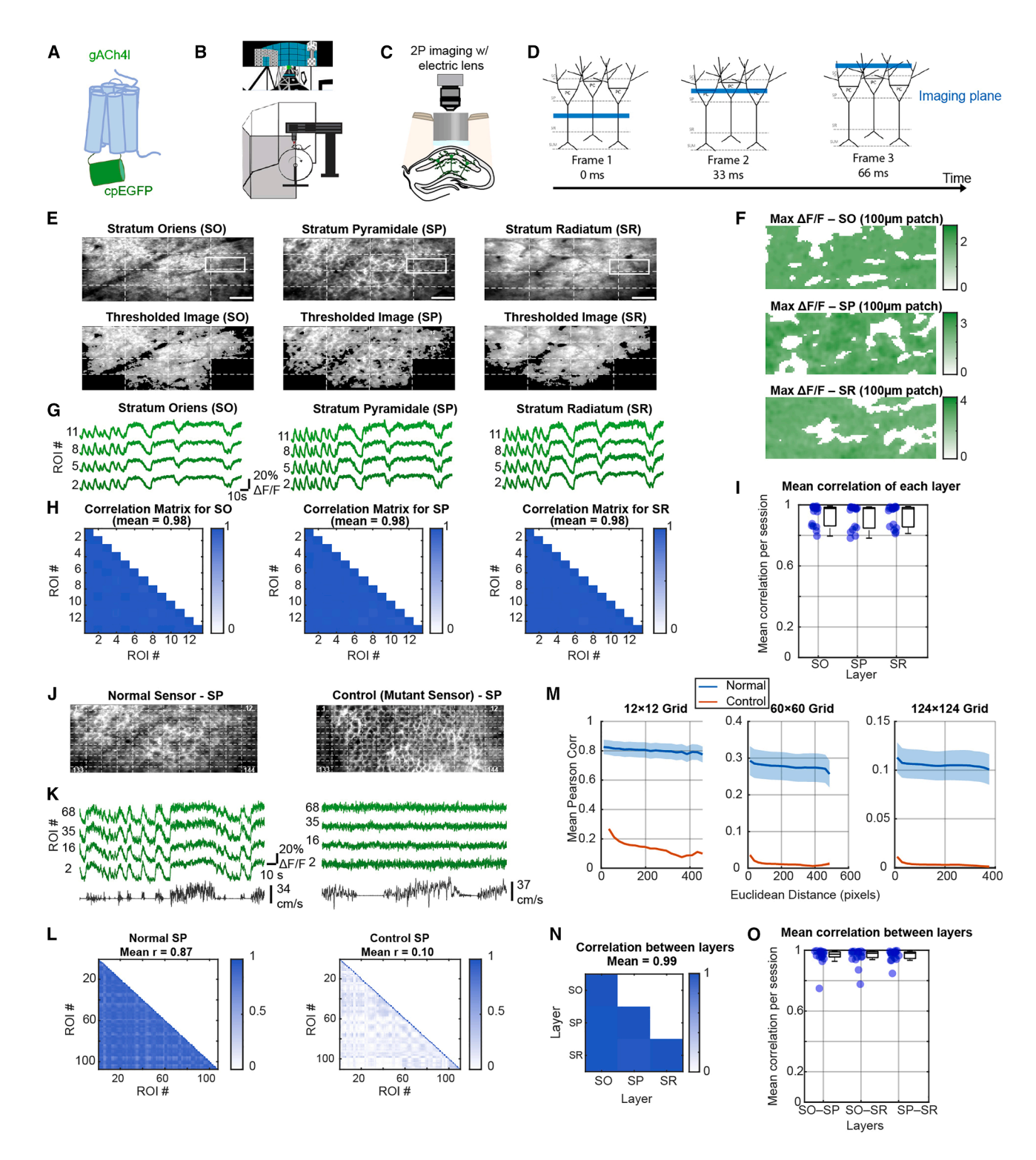


Figure 1. ACh release dynamics in CA1 of the mouse hippocampus are spatially homogeneous on the hundreds of microns scale within layers and highly correlated between layers

- (A) Structure of GRAB-ACh4I, the genetically encoded ACh fluorescent sensor used here.
- (B) Diagram of experimental recording setup with head-fixed mouse on a linear treadmill (bottom) and a view down the virtual linear track (top).
- (C) Diagram of the hippocampal window used for functional recordings of CA1 with 2P combined with an electric lens for rapid focal plane changing.
- (D) Schematic representation of 2P time-series acquisition using electric lens for focal plane switching after each frame acquisition (~10 Hz).



combined with two-photon imaging and a virtual reality (VR) system to investigate the spatiotemporal pattern of ACh release in mouse hippocampal CA1. We determined the ACh release patterns at micron spatial and sub-second temporal resolution while mice navigated in VR. Moreover, we co-recorded ACh release patterns and place cell firing in CA1 populations to establish the relationship among ACh release, the hippocampal code for space, and behavioral states. Finally, we used scopolamine, a muscarinic antagonist, to determine the effects of administration on spatial behaviors in VR and the associated hippocampal code for space.

RESULTS

ACh release dynamics in CA1 of the mouse hippocampus are spatially homogeneous on the hundreds of microns scale within layers and highly correlated between layers

We first asked how homogeneous or heterogeneous changes in ACh release are across the hippocampus of behaving mice. The projection patterns from the basal forebrain to CA1 are known to be highly laminar specific, with CA1 pyramidal layer (stratum pyramidale, SP) receiving ACh inputs almost exclusively from the vertical limb of the diagonal band of Broca (VDB) whereas stratum oriens (SO) and stratum radiatum (SR) receives ACh inputs from the medial septum (MS) and VDB. A rabies tracing study also showed CA1 excitatory neurons in SP received greater ACh innervation compared to CA1 inhibitory neurons in SO. Thus, these laminar-specific cholinergic projection patterns could generate heterogeneity in ACh release dynamics across CA1 layers during behavior, but no measurements have been made to examine this possibility.

Measurements of ACh release with high spatiotemporal resolution have been made possible by the development of genetically encoded fluorescent ACh sensors. ^{19,20} While GRAB-ACh (GPCR-activation-based ACh) sensors have enabled measurement of ACh dynamics in cortex using high-resolution two-photon imaging, ^{21,22} and in hippocampus using single point bulk fluorescence fiber photometry, ¹² the spatial distribution and layer-specific patterns of hippocampal ACh release have

not been characterized with two-photon imaging in the hippocampus. To investigate how homogeneous or heterogeneous the spatiotemporal ACh release is in CA1 both on the fine scale within imaging fields and across layers of CA1, we utilized two-photon microscopy with an electric lens, 23 which rapidly switched between focal planes in SO, SP, and SR. We expressed GRAB-ACh4l (EC50 6.6 μM ; see STAR Methods), which was improved based on GRAB-ACh3 20 (EC50 2.2 μM) (Figure 1A), in CA1 neurons through AAV viral injections and implanted a chronic hippocampal window above the viral-injected region of CA1 (Figure 1C).

We co-acquired time-series movies of GRAB-ACh4l fluorescence of SO, SP, and SR in CA1 while mice were traversing a virtual linear track (Figures 1B and 1D). The SO and SR imaging fields were 65 \pm 10 μ m dorsal and ventral of the SP imaging field. We imaged \sim 400 μ m \times 400 μ m fields of view in SO, SP, and SR layers. To investigate the spatiotemporal similarity of ACh release within these imaging fields of view, we divided the imaging fields into different size square small fields (or regions of interest [ROIs]; 4×4 , 12×12 , 60×60 , and 124×124 grids with ROIs of 100 μm \times 100 $\mu m,$ 33 μm \times 33 $\mu m,$ 6.6 μm \times 6.6 $\mu m,$ and 3.2 $\mu m \times$ 3.2 $\mu m,$ respectively), extracted the GRAB-ACh4l $\Delta F/F$ vs. time trace (ACh release) for each ROI and computed the Pearson correlation between each pair of ROIs (example 4×4 grid, Figures 1E and 1G). The mean (±SEM) correlation coefficients of the SO, SP, and SR are 0.92 \pm 0.02, 0.91 \pm 0.02, and 0.92 \pm 0.02 (example 4 \times 4 grid, Figures 1H and 1I; example 12 \times 12 grid, Figures 1J-1L). When we examined the mean correlation between the ROIs as a function of the distance between them, we found largely uniform correlations across distance (Figure 1M); the small decrease in correlation across distance is likely due to small amounts of residual motion noise, which is locally more coherent. We also made mean (and max) $\Delta F/F$ images of our fields of view so that we could visualize any heterogeneity at small scales (see Figure 1F) but again found relatively uniform ACh signaling. This is consistent with homogeneous ACh signaling across our fields of view, with a resolution down to about 3 µm (see Figures 1F and 1M). These $\Delta F/F$ images were consistent with the above correlation analysis, indicating largely homogeneous ACh signaling across our fields of view. Thus, within each

⁽E) Example 2P images of GRAB-ACh4l labeled CA1 regions at the indicated layers (E), with an overlaid DASHED grid showing 16 ROIs. Dim pixels below an intensity threshold were masked out (black regions). Scale bar: 50 μm.

⁽F) Maximum GRAB-ACh4l ΔF/F image (max over recording session for each pixel) of solid rectangle regions shown in (E).

⁽G) GRAB-ACh4l Δ F/F (ACh release) vs. time traces from selected ROIs in (E).

⁽H) Matrix of Pearson correlation coefficients calculated between the GRAB-ACh4l Δ F/F vs. time traces shown in (E) and (G) for each pair of ROIs within each layer's imaging field for SO, SP, and SR, respectively; from example dataset shown in (E) and (G). Note that only ROIs with more than half of pixels above the intensity threshold were included (13 out of 16 ROIs).

⁽I) Mean correlation of GRAB-ACh4l Δ F/F vs. time traces across the (included) ROIs within each layer (as seen in H). Each point represents the mean from a separate dataset (N = 4 mice, 18 FOVs for each layer). Box whisker plot for each layer: mean \pm STD.

⁽J) Same as (E, top) but with 144 ROIs. Left, functional GRAB-ACh4l; right, non-functional mutant sensor.

⁽K) Same as (G) but for ROIs from (J). Left, functional GRAB-ACh4I; right, non-functional mutant sensor. Running speed of mouse shown in black.

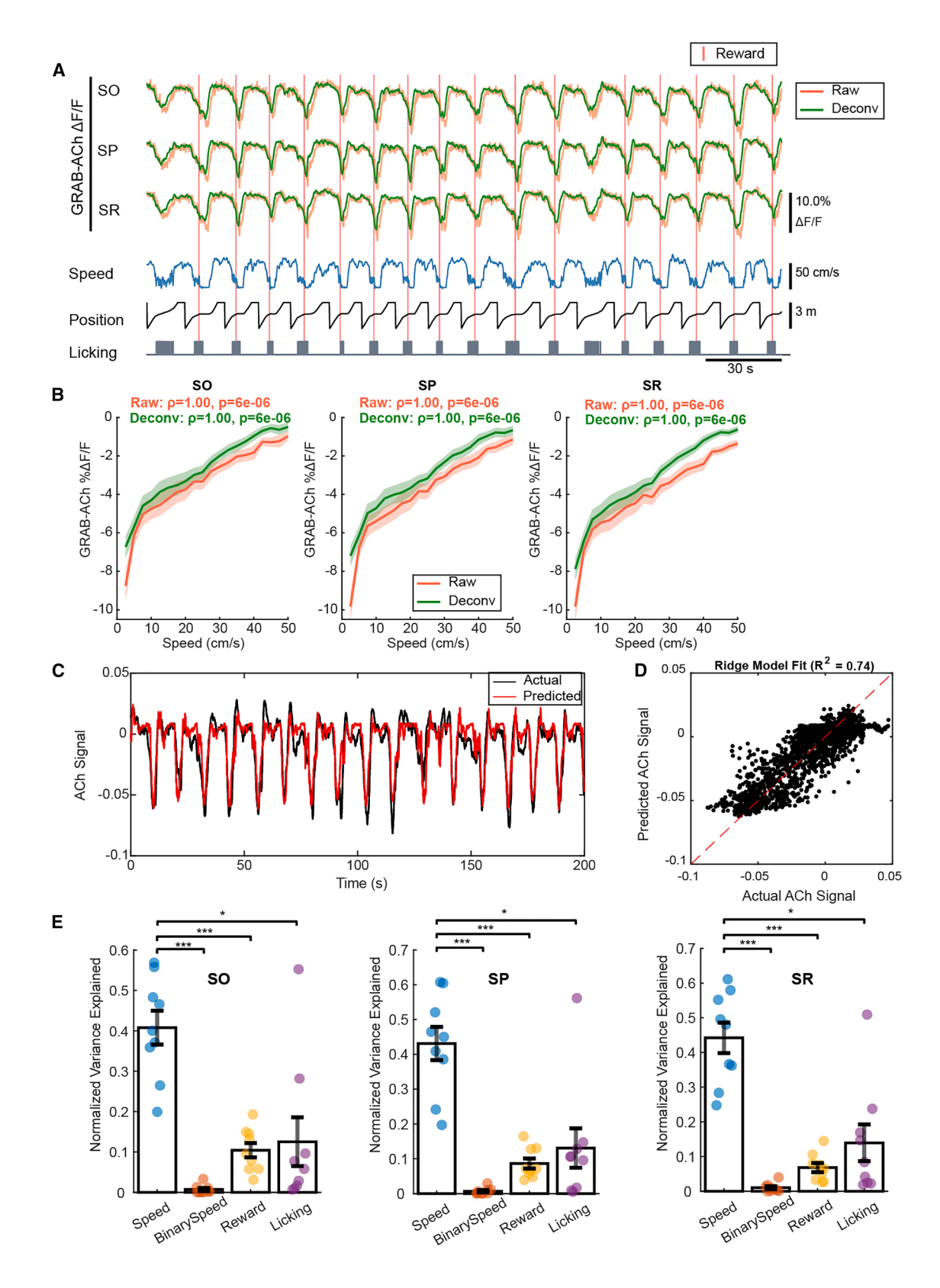
⁽L) Same as (H) but for ΔF/F vs. time traces shown in (J) and (K). Left, functional GRAB-ACh4l; right, non-functional mutant sensor.

⁽M) Mean correlation between ROIs as a function of the Euclidean distance between them, for grid sizes of 12×12 , 60×60 , and 124×124 . Mean \pm STD across FOVs (N = 4 functional sensor mice, 18 FOVs, blue; N = 2 control sensor mice, 16 FOVs, red).

⁽N) Matrix of Pearson correlation coefficients calculated between the GRAB-ACh4l Δ F/F vs. time trace average over each layer in (E) and (G) for each pair of layers; from example dataset shown in (E) and (G).

⁽O) Each point represents the Pearson correlation coefficient between indicated layers (as seen in N) from a separate dataset (N = 4 mice, 18 FOVs for each layer). Box whisker plots: mean ± STD.





(legend on next page)

Article



layer of CA1, the temporal correlations of ACh signaling are highly correlated across hundreds of microns, with a resolution down to ${\sim}3~\mu m.$

As a control, we used an activity-independent GRAB-ACh variant (STAR Methods), trained mice to perform the same VR task, and collected imaging data and performed analysis in an identical way to the functional sensor datasets. The control Δ F/F vs. time traces showed no signal transients (Figures 1J and 1K), and correlation coefficients between ROIs within layers were significantly lower than the functional sensor correlations (Figures 1L and 1M).

We then computed correlation coefficients of the whole-frame average GRAB-ACh4l $\Delta F/F$ vs. time traces of each layer. The mean ($\pm SEM$) correlation coefficients between pairs of each layer are 0.96 \pm 0.01 for SO-SP, 0.96 \pm 0.01 for SO-SR, and 0.97 \pm 0.01 for SP-SR (Figures 1N and 10), indicating that ACh release is also highly correlated across SO, SP, and SR in CA1. Taken together, these results indicate that ACh release dynamics in CA1 of the mouse hippocampus are spatially homogeneous across volumes spanning hundreds of microns, with a resolution down to $\sim \! 3~\mu m$ within layers.

ACh release in CA1 is positively correlated with the running speed of the mouse across hippocampal layers

Having observed that the spatiotemporal dynamics of ACh release in CA1 are highly homogeneous, we then sought to establish the relationship between ACh release patterns and behavior in mice performing spatial navigation tasks. ACh release in the hippocampus measured using microdialysis has been shown to be coarsely positively correlated with spontaneous motor activity. 11,24 However, microdialysis can only resolve change in ACh release on the timescale of tens of minutes, which is considerably slower than changes in an animal's motor activity. Recent studies using GRAB-ACh3.0 combined with fiber photometry to record ACh release in CA1 of freely moving mice have confirmed this positive correlation between ACh release and locomotion speed with seconds-scale resolution. 12,25 Similarly, population activity of MS cholinergic neurons (measured using calcium indicators) closely tracks changes in locomotor speed in behaving mice.²⁶ However, ACh release dynamics have not been characterized in the hippocampus of head-fixed mice performing a virtual linear track navigation task.

Thus, we trained mice to traverse a 3-m long virtual linear track to collect water rewards with a reward probability of 80% for each run. After the mice reached the performance criteria (see STAR Methods), we imaged ACh release in CA1 with the same multiplane two-photon imaging setup as described above. Since

GRAB-ACh4l Δ F/F vs. time in CA1 were homogeneous across location, we computed the average Δ F/F (ACh release) from the whole frame for each layer. We observed highly dynamic ACh release in SO, SP, and SR layers of CA1 when mice were performing the task, which seemed to be correlated with running speed (Figures 2A and S1). Before performing analysis to relate ACh release to behavior, we first deconvolved the average Δ F/F vs. time traces using 0.06 s activation kernel and 1 s decay (inactivation) kernel (from *in vivo* measurements; Figure S2; STAR Methods); these deconvolved traces were used for all subsequent analysis.

Since ACh release could relate to other behavioral and task variables in addition to running speed, we next implemented a generalized linear model (GLM) using running speed, licking, time relative to reward, and running state (0 if below 0.5 cm/s and 1 if above) as predictors and parsed their contributions to the ACh release signal across hippocampal layers. This analysis revealed that running speed explained the most variance in the ACh signal, significantly exceeding that explained by the other predictors (Figures 2C–2E). While we found that a small amount of variance was explained by reward time and licking, running speed was the dominant determinant of ACh signaling in the hippocampus during a virtual linear track navigation task. Based on this result, we focused our analysis on the relationship between speed and ACh release.

To quantify the relationship between ACh release and speed, we next binned GRAB-ACh Δ F/F by speed by computing the mean GRAB-ACh Δ F/F in each speed bin (2.5 cm/s per bin). We observed that ACh release was positively correlated with speed, and these correlations were highly similar across the three layers of CA1 (Figure 2B; Spearman's rank correlation—SO, $\rho =$ 1.00, $p = 6.0 \times 10^{-6}$; SP, $\rho = 1.00$, $p = 6.0 \times 10^{-6}$; SR, $\rho = 1.00$, $p = 6.0 \times 10^{-6}$). We also analyzed ACh release dynamics between rewarded and non-rewarded (catch) trials in VR (Figure S3A) and in mice spontaneously running in the dark with no task (no VR; Figures S3B and S3C) and found highly similar results of a positive correlation between ACh release and running speed. Thus, across hippocampal CA1 layers in mice performing a spatial task in a familiar environment, running speed is the dominant behavioral variable explaining ACh release variance, and this ACh release is positively correlated with running speed.

During exposure to a novel environment, ACh release in CA1 persistently increased while maintaining positive speed correlation

After establishing the spatiotemporal ACh release patterns in mice exploring a familiar environment, we next asked how ACh release

Figure 2. ACh release in CA1 is positively correlated with the running speed of the mouse across hippocampal layers

(A) Example linear track navigation recording session showing GRAB-ACh4l Δ F/F vs. time traces (raw original Δ F/F traces in red, deconvolved with a 0.06 s activation kernel and 1 s decay [inactivation] kernel in green) for SO, SP, SR, mouse running speed, position along 3 m track, and licking.

- (B) Relationship between ACh release and speed for each layer: GRAB-ACh Δ F/F vs. time trace binned by speed (2.5 cm/s per bin, original Δ F/F in red, deconvolved in green), averaged across all sessions (N = 3 mice, 9 sessions).
- (C) Generalized linear model (GLM, red) prediction of GRAB-ACh $\%\Delta F/F$ vs. time trace (black) using running speed, licking, time relative to reward, and running state as predictors.
- (D) Time point by time point relationship between predicted and actual GRAB-ACh $\%\Delta F/F$ signal from (C).
- (E) Across SO, SP, and SR, variance of GRAB-ACh $\%\Delta F/F$ vs. time traces explained by each of the GLM predictors normalized by total variance explained in each session (N = 3 mice, 9 sessions; mean \pm SEM; $^*p < 0.05$; $^{***}p < 0.01$; Kruskal-Wallis test).



patterns change during novel environment exposure and new spatial memory formation in CA1. ACh has long been thought to play an important role in memory encoding and consolidation by regulating the flow of information between the hippocampus and neocortex. ^{1,13} A theoretical framework had proposed that high ACh sets the circuit dynamics for memory encoding by selectively allowing sensory information from the cortex to reach the hippocampus (notably the dentate gyrus [DG] and region CA3), whereas low ACh configures the circuit dynamic for memory consolidation by weakening the influence of the cortical input to the hippocampus and strengthening hippocampal efferents to the cortex. ^{7,8} However, changes in ACh release during a novel environment exposure, where spatial memory formation is taking place, are poorly understood since no direct measurements of ACh release with high-spatial and high-temporal resolution have been made.

To determine whether ACh release in CA1 changes during novel environment exposure, we used a VR environment switch paradigm, which has been shown to cause global remapping in CA1.²⁷ Mice were first trained to traverse a virtual linear track to collect water rewards until they reach the performance criteria before imaging experiments. In the imaging session, mice ran in the familiar environment for at least 25 laps before being suddenly switched into a novel environment (Figure 4A). Mice then explored the novel environment for at least 25 laps before the imaging session ended. Interestingly, switching to the novel environment caused a rapid increase of ACh release that appeared across all layers of CA1 and lasted dozens of laps in the novel environment (Figure 3A). To test whether the increase of ACh release was due to differences in mouse speed profiles in the novel environment compared to the familiar environment, we binned GRAB-ACh Δ F/F by speed (0–50 cm/s, 2.5 cm/s per bin) and computed the mean ΔF/F in each bin. The novel environment switch caused a marked overall increase of ACh release across all speeds; this was evident from just after the switch, lasted for dozens of laps, and appeared across all three layers of CA1 (Figures 3B and 3C). In the example session shown in Figure 3A, the increase of ACh release persisted even after the \sim 20th laps in the novel environment, particularly in the SO and SP layer (Figure 3B). A similar increase in ACh release can be seen across all layers from the pooled results from all sessions (Figure 3C). In the novel environment, ACh release and speed still maintained a positive correlation, though with a reduced slope compared to the familiar environment (Figure 3C). We also used our GLM analysis to address the question of whether changes in behavior could account for the increases in ACh release observed in novel environments. A GLM trained on behavior immediately before the environment switch failed to predict the subsequent increase in ACh release in the novel environment, indicating that behavioral changes alone cannot explain this increase (Figure S4). Taken together, these results establish that exposure to a novel environment causes a rapid and persistent increase in ACh release in CA1 that is not explained by mouse speed profile changes.

The magnitude of speed-correlated ACh release decreases during voluntary task disengagement, accompanied by less precise and reliable place maps

Having observed the highly dynamic ACh release when mice were actively engaged in a spatial task, we next asked how ACh release is modulated by different behavioral states. ACh release from the widespread cholinergic projection is associated with arousal, task engagement, and attentional brain states ^{13,21,28}; however, whether and how ACh release specifically in the hippocampus is modulated by behavioral engagement is poorly understood. To address this question, we recorded ACh release during engaged and disengaged portions of individual sessions. In these mice, CA1 neurons were therefore labeled with GRAB-ACh4l, but they were also labeled with jRGECO1a (a red calcium indicator) (Figures 4A–C), allowing us to co-record ACh release and place cell firing in the pyramidal layer (SP) during the same sessions—a capability we make use of below.

First, we addressed the relationship between ACh release and task engagement. To induce voluntary disengagement in the linear track task (see STAR Methods for behavior criteria; Figure S5), we allowed mice to traverse a familiar environment with large reward size for a prolonged period of time (usually > 1 hr) to the point where they were satiated with water rewards. In the early part of such sessions, mice slowed down (speed close to 0 cm/s) and showed anticipatory licking before the reward delivery, which were indications of an actively engaged state. Toward the end of the sessions, mice displayed behavioral signatures of a disengaged state, in which they slowed down less before the reward location and showed less anticipatory licking (Figures 4D and 4E). ACh release in the engaged vs. disengaged periods were also markedly different (Figure 4D), with fewer and lower magnitude changes in release apparent in example disengaged vs. engaged periods of the sessions. To quantify the changes in ACh release across the periods, we again binned GRAB-ACh ΔF/F by speed bins and computed the mean $\Delta F/F$ for each speed bin (Figure 4F). Across all mice, we found that the magnitude of ACh release across the speed range was significantly reduced in the disengaged period compared to the engaged period (Figure 4G; mean amplitude of GRAB-ACh4l Δ F/F, engaged, 9.70% \pm 0.57% Δ F/F; disengaged, $4.96\% \pm 0.33\% \Delta F/F$; p value = 2.44×10^{-4} ; Wilcoxon signed-rank test). We also used our GLM analysis to address the question of whether changes in behavior could account for the decrease in ACh release magnitude observed in the disengaged condition and found that such behavior changes could not account for the magnitude decrease (Figure S5). Further, as a control, we also quantified the speed correlation of ACh release across sessions spanning the same amount of time but where mice were given regular size (not large) water rewards and thus did not become satiated and disengaged. We found that the magnitude of the speed-correlated ACh release in the ends of these sessions was not different from that of the first parts of these sessions (Figure S5). Therefore, significant changes in the magnitude of speed correlated ACh release are seen in the hippocampus across different states of task engagement.

A recent study showed that precise and reliable place cell firing in CA1 is dependent on behavioral engagement in the spatial task; when mice voluntarily disengaged from the task, the place code degraded extensively even though mice continuously traversed the environment.²⁹ Since we found significant changes in ACh release from engaged to disengaged states,



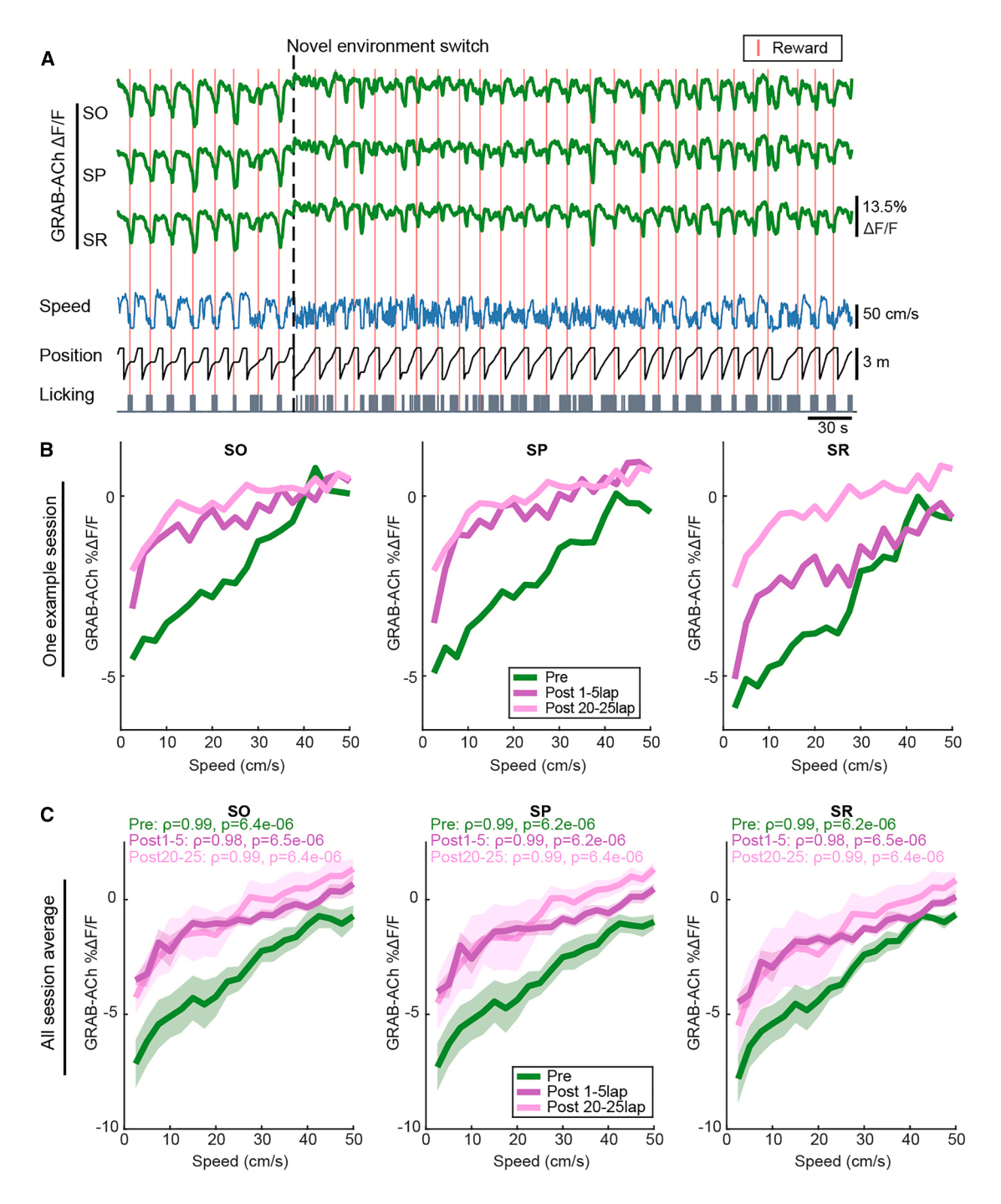
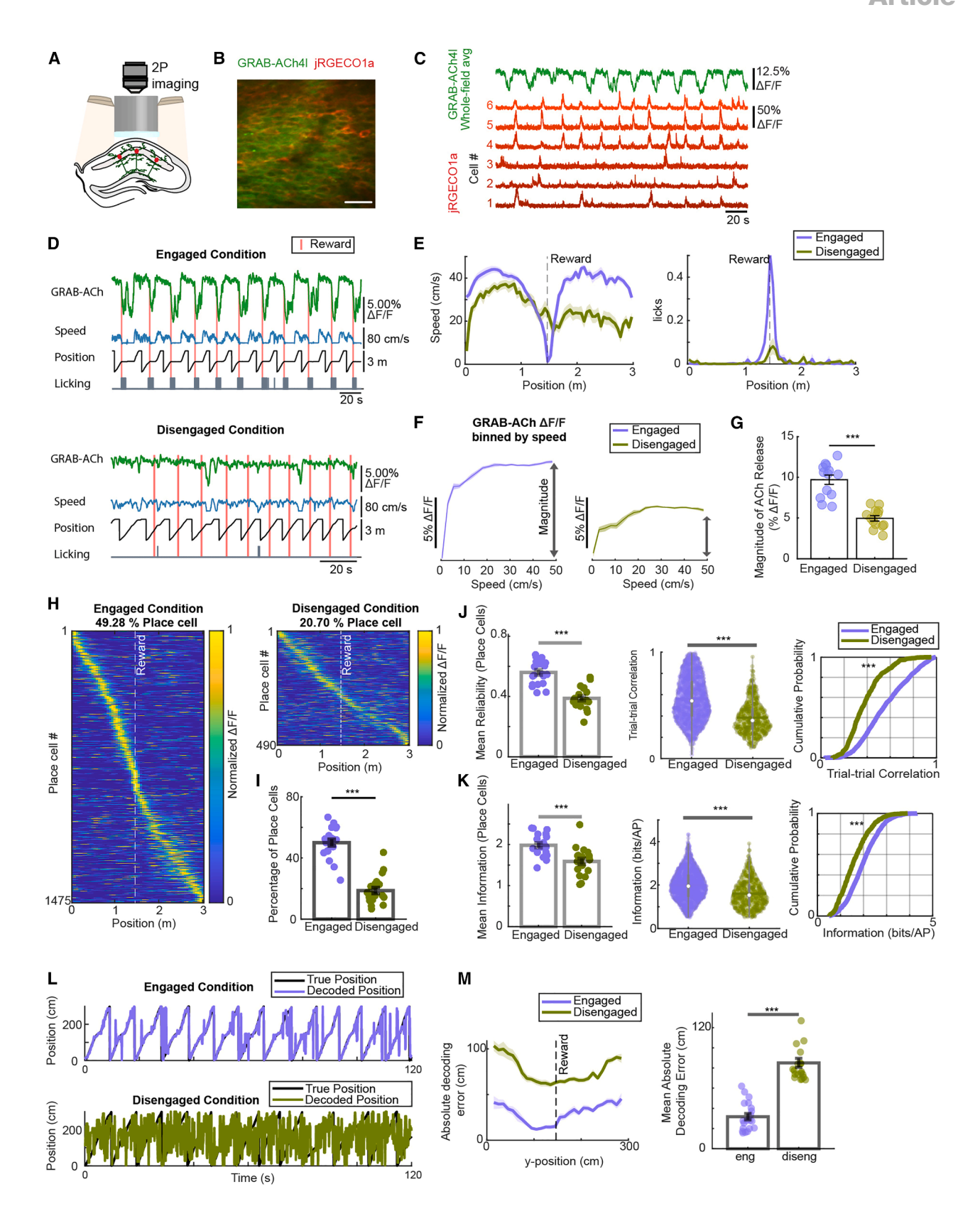


Figure 3. During novel environment exposure, ACh release in CA1 persistently increased while maintaining positive speed correlation
(A) Example linear track navigation recording session where the environment was suddenly switched from a familiar to a novel track (dashed line).
(B) ACh release vs. speed relationship for each layer from the example in (A). Colors indicate the laps that the relationship was calculated over.
(C) Same as (B) but averaged over all environment switch sessions (N = 3 mice, 6 sessions, Spearman correlation coefficient [p] and p value [p] are shown for each curve).

we wondered whether such ACh changes co-occurred with encoding changes in the place cell population. We therefore made use of the jRGECO1a place cell recordings that were acquired during the same sessions as the above ACh release recordings

across engaged and disengaged periods (Figures 4D and 4E). Interestingly, when we separately identified place cells in the engaged and disengaged periods (Figure 4H), we found a significant reduction in the percentage of cells that were place cells in





Article



the disengaged periods (Figure 4I; mean percentage of place cells per session, disengaged, 18.75% ± 2.02%; engaged, $50.05\% \pm 2.24\%$; p value = 8.86×10^{-5} , Wilcoxon signed-rank test). The place cells also appeared to have less precise place fields during the disengaged periods (Figure 4H). To quantify this observation, we computed, for each cell, the spatial correlation between the spatial firing pattern on each trial to the average over all trials. We found that this correlation (referred to as place cell firing reliability) was significantly lower during disengaged periods (Figure 4J; mean trial-trial correlation per session, disengaged, 0.39 ± 0.02 ; engaged, 0.56 ± 0.02 ; p value = 1.89×10^{-4} ; Wilcoxon signed-rank test). Further, the spatial information of place cells was also significantly lower during the disengaged periods (Figure 4K; mean place cell spatial information per session, disengaged, 1.56 \pm 0.07 bits/AP; engaged, 1.98 \pm 0.06 bits/AP; p value = 2.93×10^{-4} ; Wilcoxon signed-rank test). Lastly, we applied a Bayesian decoding approach to examine spatial coding accuracy at the population level (including both place and non-place cells). Decoding accuracy was markedly lower for the disengaged periods, and the absolute decoding error was higher across the length of the track (Figures 4L and M; mean absolute decoding error per session, disengaged, 85.12 ± 4.47 cm; engaged, 31.74 ± 3.16 cm; p value = 8.86×10^{-5} ; Wilcoxon signed-rank test). Overall, we found that when mice voluntarily disengaged from the spatial task, the magnitude of running speed correlated ACh release decreased, and this was accompanied by a reduction in the number of place cells and less precise place maps.

Administration of scopolamine mimics the effects of voluntary disengagement in terms of behavior and place cell metrics

Across brain areas, muscarinic receptors have been shown to be involved in the modulation of attention. Scopolamine, a commonly used muscarinic receptor antagonist, can induce attentional impairments in humans that result in failure in detecting cues in attentional tasks.³⁰ In the spatial navigation context, rats and humans that were administered scopolamine performed worse in a hidden-goal task.¹⁶ Recording of place cell firing in rats with intracerebroventricular scopolamine application (blocking muscarinic receptors throughout the brain) revealed that place firing specificity degrades and firing rates reduce³¹ (reduced CA1 firing rate also seen in mice with i.p. scopolamine injections³²). This effect was also observed in follow-up studies with local hippocampal scopolamine application, and additional pharmacology showed this effect is likely mediated by the blockade of the postsynaptic M1 receptor as well as the presynaptic M2 and M4 receptors in CA1.33-35 However, it is largely unknown how hippocampal place cell firing patterns change in relation to the changes in spatial navigation abilities induced by scopolamine administration.

To investigate these questions, we systemically administered a high dose (1 mg/kg) or a low dose (0.5 mg/kg) of scopolamine (or saline as control) to mice through intraperitoneal injections prior to each imaging session. We then imaged ACh release with GRAB-ACh4l and place cell firing with jRGECO1a as mice traversed a familiar linear track. The high dose of scopolamine caused drastic changes in running and licking behaviors compared to saline (Figure 5A), which appeared as overall slower speed across the track, and far less deceleration and anticipatory licking before the reward location (Figure 5B). Consistently, the low dose of scopolamine had a milder effect on running and licking behavior compared to saline (Figures 5A and 5B), with an overall slower speed across the track (similar to high scopolamine) and less deceleration and anticipatory licking before the reward location (though more than high scopolamine). Interestingly, the effects of high-dose scopolamine on running and licking behavior were highly similar to

Figure 4. The magnitude of speed-correlated ACh release decreases during voluntary task disengagement, accompanied by less precise and reliable place maps

- (A) Schematic showing CA1 neurons labeled with both GRAB-ACh4l and jRGECO1a.
- (B) Example field of CA1 neurons labeled with both GRAB-ACh4l (green) and jRGECO1a (red). Scale bar: 50 μm.
- (C) Example GRAB-ACh4l (green, whole-frame average) and jRGECO1a $\Delta F/F$ (red, selected cells) vs. time traces co-recorded from the same field of view.
- (D) Example linear track navigation recording session showing the period when the mouse is engaged (top) vs. disengaged (bottom) from the task.
- (E) Plot of mouse speed vs. position (left) and licking vs. position (right) around the reward location for engaged (purple) and disengaged (yellow) periods. Averaged over all mice and sessions (N = 5 mice, 20 sessions for each condition).
- (F) ACh release vs. speed relationship for engaged (purple) and disengaged (yellow) periods, representing the exemplary session shown in (D).
- (G) Each point represents the magnitude of ACh release across the speed range (ACh release at 50 cm/s to ACh release at 2.5 cm/s) for each engaged vs. disengaged period of each session (N = 5 mice, 20 sessions for each condition). Box whisker plot for each condition: mean \pm SEM; ***p < 0.01 (Wilcoxon signed-rank test).
- (H) Mean jRGECO1a Δ F/F vs. track position for all place cells during engaged periods (left) or disengaged periods (right) (cross-validated; N = 5 mice, 20 sessions for each condition).
- (I) Each point represents the percentage of jRGECO1a ROIs identified as place cells for each engaged vs. disengaged period of each session (N = 5 mice, 20 sessions for each condition). Box whisker plot for each condition: mean ± SEM; ***, p < 0.01.
- (J) Spatial correlation between the spatial firing pattern on each trial to the average over all trials (referred to as place cell firing reliability) for every place cell (center, with cumulative sum at right) or averaged across all place cells in each engaged vs. disengaged period of each session (left; mean \pm SEM). (N = 5 mice, 20 sessions for each condition; ***p < 0.01; Wilcoxon signed-rank test).
- (K) Same as (J) but for spatial information of all place cells.
- (L) Two example plots of Bayesian decoded position vs. time showing actual position (black) and decoded position (colors) for engaged period (top) and disengaged period (bottom) (N = 5 mice, 20 sessions for each condition).
- (M) Left, decoding position error vs. track position averaged across all engaged periods (purple) and disengaged periods (yellow); right, each point represents mean absolute decoding error averaged across track position for each engaged vs. disengaged period of each session (N = 5 mice, 20 sessions for each condition; mean \pm SEM; ***, p < 0.01; Wilcoxon signed-rank test).



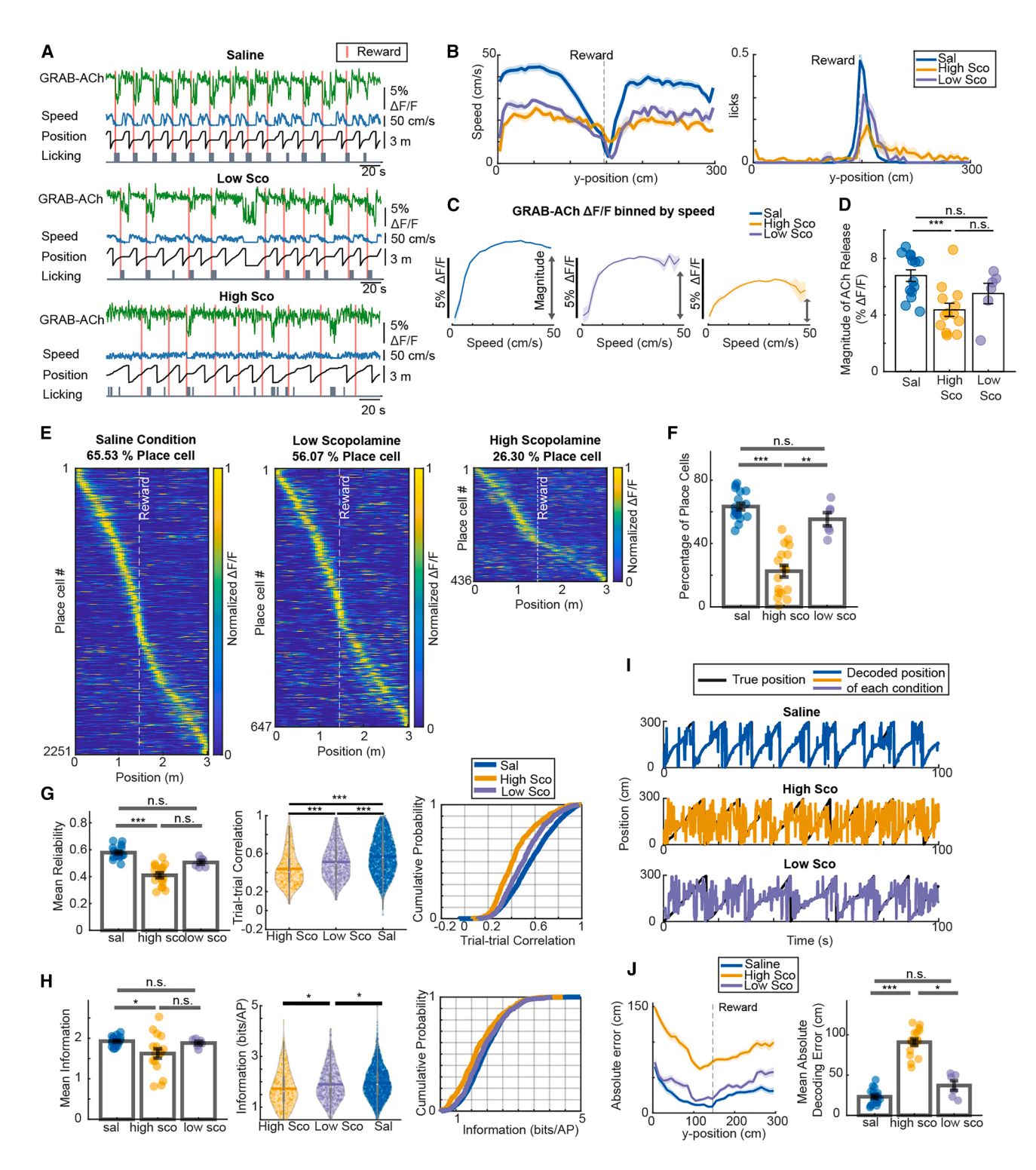


Figure 5. Administration of scopolamine mimics the effects of voluntary disengagement in terms of behavior and place cell metrics

(A) Three example linear track navigation recording sessions from mice administered a high dose of scopolamine (1 mg/kg), a low dose of scopolamine (0.5 mg/kg), or saline as control.

(B) Plot of mouse speed vs. position (left) and licking vs. position (right) around the reward location for high scopolamine, low scopolamine, and saline sessions. Averaged over all mice and sessions (saline: N = 4 mice, 17 sessions; high sco: N = 4 mice, 17 sessions; low sco: N = 2 mice, 6 sessions).

(C) ACh release vs. speed relationship for high scopolamine, low scopolamine, and saline sessions, representing the exemplary session shown in (A).

Article



that of the voluntary disengaged states described above (Figure 4). Scopolamine has been shown to block GRAB-ACh signals at very high concentrations (5–20 mg/kg). We observed a dose-dependent decrease of GRAB-ACh4I $\Delta F/F$ (Figure 5C) with systemic administration, which suggested scopolamine reached the hippocampus and was active in a dose-dependent manner (Figure 5D; mean amplitude of GRAB-ACh4I $\Delta F/F$, saline, 5.92% \pm 0.27% $\Delta F/F$; high scopolamine (sco), 4.96% \pm 0.27% $\Delta F/F$; low sco, 5.43% \pm 0.48% $\Delta F/F$; Kruskal-Wallis test with post-hoc pairwise comparisons, Kruskal-Wallis test p value = 0.02; post-hoc p value for saline and high sco = 0.02; p value for saline and low sco = 0.43; p value for low and high sco = 0.37).

Given that the effects of scopolamine mimicked the effects of voluntary disengagement in terms of behavior, we then asked whether and how the place code in CA1 was affected by scopolamine. When we separately identified place cells in the three experimental conditions (high scopolamine, low scopolamine, and saline), we found a significant reduction in the percentage of place cells in both the high and low scopolamine conditions, with the high scopolamine condition having a significantly larger effect (Figure 5F; mean percentage of place cells per session, saline, $63.35\% \pm 2.08\%$; high sco, $22.51\% \pm 3.70\%$; low sco, 55.27% ± 4.17%; Kruskal-Wallis test with post-hoc pairwise comparisons, Kruskal-Wallis test p value = 5.88×10^{-7} ; posthoc p value for saline and high sco = 4.59×10^{-7} ; p value for saline and low sco = 1; p value for low and high sco = 0.01). Place cells in the high scopolamine condition were also less reliable trial-to-trial (Figure 5G; mean trial-trial correlation per session, saline, 0.58 ± 0.01 ; high sco, 0.41 ± 0.02 ; low sco, 0.51 ± 0.02 ; Kruskal-Wallis test with post-hoc pairwise comparisons, Kruskal-Wallis test p value = 5.14×10^{-7} ; post-hoc p value for saline and high sco = 2.29×10^{-7} ; p value for saline and low sco = 0.10; p value for low and high sco = 0.25) and carried less spatial information compared to the saline condition (Figure 5H; mean spatial information of place cells per session, saline, 1.93 \pm 0.03 bits/AP; high sco, 1.62 \pm 0.11 bits/AP; low sco, 1.88 ± 0.04 bits/AP; Kruskal-Wallis test with post-hoc pairwise comparisons, Kruskal-Wallis test p value = 0.02; post-hoc p value for saline and high sco = 0.02; p value for saline and low sco = 1; p value for low and high sco = 0.45). Lastly, we performed Bayesian decoding to quantify the accuracy of population spatial coding and found that high scopolamine drastically increased population decoding errors, and low scopolamine resulted in similar decoding errors compared to the saline condition (Figures 5I and 5J; mean absolute decoding error per session, saline, 23.03 \pm 2.22 cm; high sco, 90.97 \pm 4.02 cm; low sco, 37.05 \pm 6.02; Kruskal-Wallis test with post-hoc pairwise comparisons, Kruskal-Wallis test p value = 2.34 \times 10 $^{-7}$; post-hoc p value for saline and high sco = 1.34 \times 10 $^{-7}$; p value for saline and low sco = 0.71; p value for low and high sco = 0.02). Taken together, systemic scopolamine administration mimicked the effects of voluntary disengagement in terms of behavior and hippocampal CA1 place cell metrics.

DISCUSSION

Our study leverages a genetically encoded ACh sensor, GRAB-ACh4I, combined with multiplane and dual-color two-photon imaging to investigate the spatiotemporal pattern of ACh release in CA1 of mice performing a spatial navigation task. We found that ACh release dynamics are largely spatially homogeneous within hippocampal layers SO, SR, and SP (Figure 1). Previous research imaging cholinergic axonal calcium transients in mouse CA1 during fear learning found relatively homogeneous responses across different axons of the same imaging field, but the population of axons responded more to aversive air-puff stimuli than other types of stimuli (tone, light).³⁶ Here, we were able to directly measure mean changes in ACh release in the extracellular space, which comprised ACh from both synaptic ("wired") and non-synaptic ("volume") transmission.³⁷ Our results provide a view of ACh release on a spatial and temporal scale not previously described and indicate that the change of extracellular ACh release is highly homogeneous on the subseconds scale and down to ${\sim}3~\mu m$ resolution. While this homogeneity supports the concept of volume transmission, 8,38 we are not able to rule out the possibility of more heterogeneous synaptic ACh release³⁹ occurring below our spatial resolution. More localized ACh changes within synaptic clefts may occur but likely would not be resolved with sufficient signal-to-noise in our measurements. We did not observe consistent spatial hotspots of ACh release, though again this could be due to limitations in

⁽D) Each point represents the magnitude of ACh release across the speed range (ACh release at 50cm/s to ACh release at 2.5cm/s) for each session of high scopolamine, low scopolamine, or saline conditions. (saline: N = 4 mice, 17 sessions; high sco: N = 4 mice, 17 sessions; low sco: N = 4 mice, 18 sessions. Box whisker plot for each condition: mean \pm SEM; ***p < 0.01; Kruskal-Wallis test.

⁽E) Mean jRGECO1a Δ F/F vs. track position for all place cells during high scopolamine, low scopolamine, and saline sessions (cross-validated; saline: N = 4 mice, 17 sessions; high sco: N = 4 mice, 17 sessions; low sco: N = 2 mice, 6 sessions).

⁽F) Each point represents the percentage of jRGECO1a ROIs identified as place cells for each high scopolamine, low scopolamine, or saline session (saline: N = 4 mice, 17 sessions; high sco: N = 4 mice, 17 sessions; low sco: N = 2 mice, 6 sessions). Box whisker plot for each condition: mean \pm SEM; ***p < 0.01; n.s., not significant; Kruskal-Wallis test.

⁽G) Spatial correlation between the spatial firing pattern on each trial to the average over all trials (place cell firing reliability) for every place cell (center, with cumulative sum at right) or averaged across all place cells in each high scopolamine, low scopolamine, or saline session (left; mean \pm SEM). (saline: N = 4 mice, 17 sessions; high sco: N = 4 mice, 17 sessions; low sco: N = 4 mice, 17 sessions; low sco: N = 4 mice, 18 sessions; low sco: N = 4 mice, 19 sessions; lo

⁽I) Three example plots of Bayesian decoded position vs. time showing actual position (black) and decoded position (colors) for a high scopolamine, low scopolamine, or saline session (saline: N = 4 mice. 17 sessions; high sco: N = 4 mice. 17 sessions; low sco: N = 2 mice. 6 sessions).

⁽J) Left, decoding position error vs. track position averaged across all high scopolamine, low scopolamine, or saline sessions; right, each point represents mean absolute decoding error averaged across track position for each high scopolamine, low scopolamine, or saline session (saline: N = 4 mice, 17 sessions; high sco: N = 4 mice, 17 sessions; low sco: N = 4 mice, 6 sessions); Box whisker plot for each condition: mean \pm SEM; $^*p < 0.05$; $^{***}p < 0.01$; n.s., not significant; Kruskal-Wallis test.



temporal and spatial resolution rather than absence of local heterogeneity. We also observed that ACh release between CA1 layers SO, SP, and SR are highly temporally correlated (Figure 1). This was surprising given that previous studies established that cholinergic inputs from the MS and VDB have laminar-specific anatomical projection patterns. Thus, although ACh input to CA1 arrives from different nuclei, the signaling patterns across these nuclei show a high level of coordination, at least for the hippocampal projecting subpopulations.

Similar to previous studies that used photometry to either record GRAB-ACh3 expressed by CA1 neurons¹² or record calcium transients in cholinergic axons in CA126 in freely behaving mice, we found that ACh release in CA1 of mouse hippocampus is positively correlated with mouse running speed in the virtual linear track (Figure 2). This correlation between ACh release and running speed has also been shown in other brain regions, such as the visual, 20-22 somatosensory, 22 and motor 22 cortex, indicating that basal forebrain cholinergic neurons are activated by locomotion and broadcast a locomotive speed signal to various brain regions by releasing ACh (though the basal forebrain also shows responses to reward, punishment, and associated cues⁴⁰ and receives inputs from subcortical nuclei related to motivation and stress⁴¹). ACh release modulated by locomotion has profound influence on neural circuit dynamics (such as in medial entorhinal cortex⁴²) and thus the brain's response to external sensory inputs. For example, locomotion can strongly enhance the visual response of primary visual cortex neurons through activating disinhibitory VIP+ interneurons, which requires nicotinic inputs from the basal forebrain.4 In the hippocampus, ACh can depolarize CA1 pyramidal neurons and alter their firing properties.⁴³ However, ACh can also alter the firing patterns of various types of interneurons through muscarinic and nicotinic receptors,44 and these in turn can up- or downregulate the firing of CA1 pyramidal neurons. Thus, the net effect of locomotion-induced ACh release on different types of CA1 neurons and the networks within the hippocampus as a whole is still largely unknown and needs to be further investigated (though see Wells et al.45).

In addition to the positive correlation between ACh release and running speed, we discovered that when mice were exposed to a novel environment, there was a marked increase in overall acetylcholine release that persisted for dozens of laps while maintaining positive speed correlation (Figure 3). This may have significant implications for understanding the signals that allow for hippocampal memory formation since multiple lines of evidence have suggested the essential role of ACh in spatial memory formation in CA1. Place cells in CA1 undergo remapping in response to changes in the animal's environment, ^{27,46} and this is thought to be one of the brain's mechanisms to form new memory representations of novel experiences that can then be decorrelated from previous experience representations.⁴⁷ Early studies using microdialysis had shown that transferring rats into a novel environment leads to increases in extracellular ACh in the hippocampus over the timescale of tens of minutes, but this experience was also accompanied by increased motor activity. Since ACh release in the hippocampus is correlated with motor activity, this posed a challenge to disambiguate whether the previously observed increase of ACh release was

due to environmental novelty, increased motor activity, or both. Our experiments and analysis were able to resolve this ambiguity and showed that the increase of ACh release during novel environment exposure cannot be explained by changes in running speed profiles. Instead, we establish that novel environment exposure causes an increase in ACh release on top of the speed-modulated ACh release dynamics. We also noted that the ACh release and speed still maintained a positive correlation in the novel environment, though with a reduced slope compared to the familiar environment. Interestingly, this is reminiscent of differences in slope of theta frequency vs. running speed observed with electrophysiology in novel versus familiar environments.

Our finding of an increase of ACh release in CA1 during novel environment exposure has several implications for functional changes in hippocampal circuitry during spatial memory formation. Slice physiology experiments showed that optogenetically induced ACh release selectively enhances excitatory-inhibitory balance and CA1 activation in the entorhinal cortex-CA1 pathway relative to the CA3-CA1 pathway, thus prioritizing novel sensory information carried by entorhinal cortex inputs to CA1⁴⁸; cholinergic modulation of presynaptic inhibition likely underlies this differential effect. 14,49 Additionally, selective immunotoxic lesioning of setpo-hippocampal cholinergic neurons affects the formation of new representations (or place cell remapping) in a novel environment, suggesting a role of the septo-hippocampal projection in regulating the processing of novel sensory information in the hippocampal network. 10 Systemic administration of scopolamine has been shown to attenuate the formation of distinct representations of new environments in CA1 of rats.⁵⁰ As described above, ACh release also regulates interneuron firing, which may reconfigure hippocampal network dynamics for memory encoding. For example, during novel environment exposure, CA1 pyramidal neurons' dendritic inhibition (from SOM+ interneurons) is transiently reduced, which is thought to create plasticity windows where regenerative events such as dendritic spikes become more prevalent and can drive synaptic plasticity to form new place fields.^{27,51} Interestingly, ACh release onto VIP+ interneurons leads to their depolarization by muscarinic receptors.⁵² Since VIP+ interneurons can inhibit downstream SOM+ interneurons, one impact of ACh release in CA1 may be to decrease the level of dendritic inhibition of pyramidal neurons⁴⁴ (i.e., VIP+ depolarization from muscarinic receptor activation leading to indirect disinhibition of pyramidal neuron dendrites via increased inhibition of SOM+ interneurons). However, SOM+ interneurons (including O-LM interneurons) are thought to receive direct cholinergic inputs and express type 1 muscarinic (M1) receptors, 53 so it is unclear how this mechanism for increased excitability might compete with the increased inhibition effect from VIP+ interneurons. Thus, the net effects of changes in Ach on hippocampal network activity and the underlying mechanisms are complicated but are an exciting area for future studies to explore.

Finally, we discovered a connection between task engagement and ACh signaling in hippocampus—when mice voluntarily disengaged from the task, the magnitude of the speed-correlated acetylcholine release decreased (Figures 4D, 4F, and 4G). ACh release has long been associated with attentional

Article



processing and is thought to support processing of extrinsic signals. ^{54,55} In the hippocampus, increased attentional demands to the spatial context and higher task performance are correlated with higher place field stability in mice, suggesting place representations in the hippocampus are gated by top-down mechanisms that depend on attention and task engagement. ⁵⁶ ACh is a strong potential candidate for such a mechanism. Computational modeling also suggests that ACh can selectively gate top-down versus bottom-up attentional processing. ⁵⁷ Our results add information to this line of reasoning by directly correlating behavioral-state-induced changes in ACh release to changes in place coding across the place cell population in CA1 (Figures 4H and 4M).

Limitations of the study

With regard to the connection between task engagement and ACh signaling in hippocampus, interestingly, we established that systemic administration of scopolamine mimics the effects of voluntary disengagement on both behavioral and place cell metrics (Figure 5). Scopolamine administration has been shown to induce attentional impairments and impact spatial navigation capabilities. 16,30 Our results provide a potential explanation for such impairments in spatial cognition-that the place code is degraded by scopolamine administration. It is important to keep in mind that this pharmacological manipulation affects numerous brain regions in addition to hippocampus, and thus it is not clear whether the reduced CA1 spatial coding is due to direct effects of altered ACh modulation in the hippocampus, in regions providing input to hippocampus, such as visual cortex and somatosensory cortex, or both. However, the concentration of scopolamine used here (0.5-1 mg/kg) is somewhat lower compared to that of previous studies^{20,58} and is below the concentration that was previously found to lead to visual acuity impairments.⁵⁸ Regardless, our results highlight the importance of muscarinic inputs to hippocampus for attentional processing and task engagement, which are likely similarly broadcast to other brain regions during spatial behavior.

While our GLM analysis provides insights into the behavioral correlates of ACh signaling, such models have inherent limitations. For example, our model does not account for the possibility that the relationship between the predictors and ACh may not be linear, and other non-linear analysis methods might better capture interactions between continuous and binary variables. While we have chosen reasonable predictors based on known correlations of ACh to behavior, it is certainly possible that other predictors (or predictor interactions) could improve the model fit. For example, while variable time lags were included for reward and licking behavior, time lags were not included for running speed, nor were interaction terms between predictors. Further, we did not explicitly model novelty or engagement and only inferred the effects of these variables through our GLM analysis.

One of our conclusions was that the magnitude of the speed correlated acetylcholine release decreased during voluntarily disengaged and that this was accompanied by a reduction in the number (and precision) of place cells. It is important to keep in mind that this finding is correlational. Future research could address this (more specifically than our scopolamine ex-

periments) by specifically manipulating ACh release in the hippocampus with optogenetics or chemogenetics and measuring changes in behavior and place cell properties.

RESOURCE AVAILABILITY

l ead contact

Requests for further information and resources should be directed to and will be fulfilled by the lead contact, Daniel Dombeck (d-dombeck@northwestern.edu).

Materials availability

All materials used in this project can be attained upon request. For additional information, or requests pertaining to resources and reagents, please reach out to the lead contact, Daniel Dombeck (d-dombeck@northwestern.edu).

Data and code availability

- All MATLAB codes used in this project can be attained upon request.
- For additional information or requests pertaining to resources and reagents please reach out to the lead contact, Daniel Dombeck (d-dombeck@northwestern.edu).
- All data reported in this paper will be shared by the lead contact upon request. Any additional information required to reanalyze the data reported in this paper is available from the lead contact upon request.

ACKNOWLEDGMENTS

This work was supported by the National Institutes of Health (NIMH R01-MH101297 to D.A.D., T32MH067564 to F.X., and 1U01NS120824 to Y.L.) and the National Natural Science Foundation of China (31925017 to Y.L.).

AUTHOR CONTRIBUTIONS

F.X. and D.A.D. planned and designed the experiments; F.X. performed experiments; G.L. and Y.L. developed GRAB-ACh4l; F.X. analyzed the data with help from D.A.D.; F.X. and D.A.D. wrote the paper with inputs and edits from G.L. and Y.L.; D.A.D. supervised all aspects of the project.

DECLARATION OF INTERESTS

Y.L. is a member of the journal's advisory board.

STAR*METHODS

Detailed methods are provided in the online version of this paper and include the following:

- KEY RESOURCES TABLE
- EXPERIMENTAL MODEL AND STUDY PARTICIPANT DETAILS
- METHOD DETAILS
 - o Mouse surgery
 - o GRAB-Ach4l
 - o Behavioral training and task in virtual reality
 - Two-photon imaging
 - o Image processing
 - o GRAB-ACh signal analysis
 - o Deconvolution of GRAB-ACh signals
 - o GLM analysis
 - O Place cell identification and analysis
 - o Behavior analysis
 - Bayesian decoding
- QUANTIFICATION AND STATISTICAL ANALYSIS





SUPPLEMENTAL INFORMATION

Supplemental information can be found online at https://doi.org/10.1016/j.celrep.2025.116443.

Received: December 18, 2024 Revised: August 20, 2025 Accepted: September 25, 2025

REFERENCES

- Hasselmo, M.E. (2006). The role of acetylcholine in learning and memory. Curr. Opin. Neurobiol. 16, 710–715. https://doi.org/10.1016/j.conb.2006. 09.002.
- Parikh, V., Kozak, R., Martinez, V., and Sarter, M. (2007). Prefrontal acetylcholine release controls cue detection on multiple timescales. Neuron 56, 141–154. https://doi.org/10.1016/j.neuron.2007.08.025.
- Picciotto, M.R., Higley, M.J., and Mineur, Y.S. (2012). Acetylcholine as a neuromodulator: cholinergic signaling shapes nervous system function and behavior. Neuron 76, 116–129. https://doi.org/10.1016/j.neuron. 2012.08.036
- Fu, Y., Tucciarone, J.M., Espinosa, J.S., Sheng, N., Darcy, D.P., Nicoll, R. A., Huang, Z.J., and Stryker, M.P. (2014). A cortical circuit for gain control by behavioral state. Cell 156, 1139–1152. https://doi.org/10.1016/j.cell. 2014.01.050.
- Disney, A.A., and Higley, M.J. (2020). Diverse Spatiotemporal Scales of Cholinergic Signaling in the Neocortex. J. Neurosci. 40, 720–725. https://doi.org/10.1523/JNEUROSCI.1306-19.2019.
- Zou, J., Gee, J.W. de, Mridha, Z., Trinh, S., Erskine, A., Jing, M., Yao, J., Walker, S., Li, Y., McGinley, M., et al. (2024). Goal-directed motor actions drive acetylcholine dynamics in sensory cortex. eLife 13, RP96931. https://doi.org/10.7554/eLife.96931.1.
- Hasselmo, M.E. (1999). Neuromodulation: acetylcholine and memory consolidation. Trends Cogn. Sci. 3, 351–359. https://doi.org/10.1016/ S1364-6613(99)01365-0.
- Hasselmo, M.E., and McGaughy, J. (2004). High acetylcholine levels set circuit dynamics for attention and encoding and low acetylcholine levels set dynamics for consolidation. Prog. Brain Res. 145, 207–231. https:// doi.org/10.1016/S0079-6123(03)45015-2.
- Giovannini, M.G., Rakovska, A., Benton, R.S., Pazzagli, M., Bianchi, L., and Pepeu, G. (2001). Effects of novelty and habituation on acetylcholine, GABA, and glutamate release from the frontal cortex and hippocampus of freely moving rats. Neuroscience 106, 43–53. https://doi.org/10.1016/ s0306-4522(01)00266-4.
- Ikonen, S., McMahan, R., Gallagher, M., Eichenbaum, H., and Tanila, H. (2002). Cholinergic system regulation of spatial representation by the hippocampus. Hippocampus 12, 386–397. https://doi.org/10.1002/hipo.1109.
- Mizuno, T., Endo, Y., Arita, J., and Kimura, F. (1991). Acetylcholine release in the rat hippocampus as measured by the microdialysis method correlates with motor activity and exhibits a diurnal variation. Neuroscience 44, 607–612. https://doi.org/10.1016/0306-4522(91)90081-x.
- Zhang, Y., Cao, L., Varga, V., Jing, M., Karadas, M., Li, Y., and Buzsáki, G. (2021). Cholinergic suppression of hippocampal sharp-wave ripples impairs working memory. Proc. Natl. Acad. Sci. USA 118, e2016432118. https://doi.org/10.1073/pnas.2016432118.
- Hasselmo, M.E., and Sarter, M. (2011). Modes and Models of Forebrain Cholinergic Neuromodulation of Cognition. Neuropsychopharmacol 36, 52–73. https://doi.org/10.1038/npp.2010.104.
- Teles-Grilo Ruivo, L.M., Baker, K.L., Conway, M.W., Kinsley, P.J., Gilmour, G., Phillips, K.G., Isaac, J.T.R., Lowry, J.P., and Mellor, J.R. (2017). Coordinated Acetylcholine Release in Prefrontal Cortex and Hippocampus Is Associated with Arousal and Reward on Distinct Timescales. Cell Rep. 18, 905–917. https://doi.org/10.1016/j.celrep.2016.12.085.

- Gedankien, T., Tan, R.J., Qasim, S.E., Moore, H., McDonagh, D., Jacobs, J., and Lega, B. (2023). Acetylcholine modulates the temporal dynamics of human theta oscillations during memory. Nat. Commun. 14, 5283. https:// doi.org/10.1038/s41467-023-41025-y.
- Laczó, J., Markova, H., Lobellova, V., Gazova, I., Parizkova, M., Cerman, J., Nekovarova, T., Vales, K., Klovrzova, S., Harrison, J., et al. (2017). Scopolamine disrupts place navigation in rats and humans: a translational validation of the Hidden Goal Task in the Morris water maze and a real maze for humans. Psychopharmacology (Berl) 234, 535–547. https://doi. org/10.1007/s00213-016-4488-2.
- Nyakas, C., Luiten, P.G., Spencer, D.G., and Traber, J. (1987). Detailed projection patterns of septal and diagonal band efferents to the hippocampus in the rat with emphasis on innervation of CA1 and dentate gyrus. Brain Res. Bull. 18, 533–545. https://doi.org/10.1016/0361-9230(87) 90117-1
- Sun, Y., Nguyen, A.Q., Nguyen, J.P., Le, L., Saur, D., Choi, J., Callaway, E. M., and Xu, X. (2014). Cell-Type-Specific Circuit Connectivity of Hippocampal CA1 Revealed through Cre-Dependent Rabies Tracing. Cell Rep. 7, 269–280. https://doi.org/10.1016/j.celrep.2014.02.030.
- Jing, M., Zhang, P., Wang, G., Feng, J., Mesik, L., Zeng, J., Jiang, H., Wang, S., Looby, J.C., Guagliardo, N.A., et al. (2018). A genetically encoded fluorescent acetylcholine indicator for in vitro and in vivo studies. Nat. Biotechnol. 36, 726–737. https://doi.org/10.1038/nbt.4184.
- Jing, M., Li, Y., Zeng, J., Huang, P., Skirzewski, M., Kljakic, O., Peng, W., Qian, T., Tan, K., Zou, J., et al. (2020). An optimized acetylcholine sensor for monitoring in vivo cholinergic activity. Nat. Methods *17*, 1139–1146. https://doi.org/10.1038/s41592-020-0953-2.
- Lohani, S., Moberly, A.H., Benisty, H., Landa, B., Jing, M., Li, Y., Higley, M. J., and Cardin, J.A. (2022). Spatiotemporally heterogeneous coordination of cholinergic and neocortical activity. Nat. Neurosci. 25, 1706–1713. https://doi.org/10.1038/s41593-022-01202-6.
- Neyhart, E., Zhou, N., Munn, B.R., Law, R.G., Smith, C., Mridha, Z.H., Blanco, F.A., Li, G., Li, Y., McGinley, M.J., et al. (2024). Cortical acetylcholine dynamics are predicted by cholinergic axon activity and behavior state. Preprint at bioRxiv. https://doi.org/10.1101/2023.11.14.567116.
- Sheffield, M.E.J., and Dombeck, D.A. (2015). Calcium transient prevalence across the dendritic arbour predicts place field properties. Nature 517, 200–204. https://doi.org/10.1038/nature13871.
- 24. Day, J., Damsma, G., and Fibiger, H.C. (1991). Cholinergic activity in the rat hippocampus, cortex and striatum correlates with locomotor activity: An in vivo microdialysis study. Pharmacol. Biochem. Behav. 38, 723–729. https://doi.org/10.1016/0091-3057(91)90233-R.
- Zhang, Y., Karadas, M., Liu, J., Gu, X., Vöröslakos, M., Li, Y., Tsien, R.W., and Buzsáki, G. (2024). Interaction of acetylcholine and oxytocin neuromodulation in the hippocampus. Neuron 112, 1862–1875.e5. https://doi. org/10.1016/j.neuron.2024.02.021.
- Kopsick, J.D., Hartzell, K., Lazaro, H., Nambiar, P., Hasselmo, M.E., and Dannenberg, H. (2022). Temporal dynamics of cholinergic activity in the septo-hippocampal system. Front. Neural Circuits 16, 957441. https:// doi.org/10.3389/fncir.2022.957441.
- Sheffield, M.E.J., Adoff, M.D., and Dombeck, D.A. (2017). Increased Prevalence of Calcium Transients across the Dendritic Arbor during Place Field Formation. Neuron 96, 490–504.e5. https://doi.org/10.1016/j.neuron. 2017.09.029.
- Thiele, A., and Bellgrove, M.A. (2018). Neuromodulation of Attention. Neuron 97, 769–785. https://doi.org/10.1016/j.neuron.2018.01.008.
- Pettit, N.L., Yuan, X.C., and Harvey, C.D. (2022). Hippocampal place codes are gated by behavioral engagement. Nat. Neurosci. 25, 561–566. https://doi.org/10.1038/s41593-022-01050-4.
- Dunne, M.P., and Hartley, L.R. (1986). Scopolamine and the control of attention in humans. Psychopharmacology (Berl) 89, 94–97. https://doi. org/10.1007/BF00175197.

Article



- Brazhnik, E.S., Muller, R.U., and Fox, S.E. (2003). Muscarinic blockade slows and degrades the location-specific firing of hippocampal pyramidal cells. J. Neurosci. 23, 611–621. https://doi.org/10.1523/JNEUROSCI.23-02-00611.2003.
- Zhou, H., Neville, K.R., Goldstein, N., Kabu, S., Kausar, N., Ye, R., Nguyen, T.T., Gelwan, N., Hyman, B.T., and Gomperts, S.N. (2019). Cholinergic modulation of hippocampal calcium activity across the sleep-wake cycle. eLife 8, e39777. https://doi.org/10.7554/eLife.39777.
- Dasari, S., and Gulledge, A.T. (2011). M1 and M4 receptors modulate hippocampal pyramidal neurons. J. Neurophysiol. 105, 779–792. https://doi. org/10.1152/jn.00686.2010.
- Gulledge, A.T., and Kawaguchi, Y. (2007). Phasic cholinergic signaling in the hippocampus: functional homology with the neocortex? Hippocampus 17, 327–332. https://doi.org/10.1002/hipo.20279.
- Brazhnik, E., Borgnis, R., Muller, R.U., and Fox, S.E. (2004). The effects on place cells of local scopolamine dialysis are mimicked by a mixture of two specific muscarinic antagonists. J. Neurosci. 24, 9313–9323. https://doi. org/10.1523/JNEUROSCI.1618-04.2004.
- Lovett-Barron, M., Kaifosh, P., Kheirbek, M.A., Danielson, N., Zaremba, J. D., Reardon, T.R., Turi, G.F., Hen, R., Zemelman, B.V., and Losonczy, A. (2014). Dendritic inhibition in the hippocampus supports fear learning. Science 343, 857–863. https://doi.org/10.1126/science.1247485.
- Sarter, M., Parikh, V., and Howe, W.M. (2009). Phasic acetylcholine release and the volume transmission hypothesis: time to move on. Nat. Rev. Neurosci. 10, 383–390. https://doi.org/10.1038/nrn2635.
- Descarries, L., Mechawar, N., Aznavour, N., and Watkins, K.C. (2004).
 Structural determinants of the roles of acetylcholine in cerebral cortex.
 In Progress in Brain Research Acetylcholine in the Cerebral Cortex (Elsevier), pp. 45–58. https://doi.org/10.1016/S0079-6123(03)45002-4.
- Frotscher, M., and Léránth, C. (1985). Cholinergic innervation of the rat hippocampus as revealed by choline acetyltransferase immunocytochemistry: A combined light and electron microscopic study. J. Comp. Neurol. 239, 237–246. https://doi.org/10.1002/cne.902390210.
- Hegedüs, P., Sviatkó, K., Király, B., Martínez-Bellver, S., and Hangya, B. (2022). Cholinergic activity reflects reward expectations and predicts behavioral responses. iScience 26, 105814. https://doi.org/10.1016/j. isci. 2022. 108814.
- 41. Hu, R., Jin, S., He, X., Xu, F., and Hu, J. (2016). Whole-Brain Monosynaptic Afferent Inputs to Basal Forebrain Cholinergic System. Front. Neuroanat. 10, 98. https://doi.org/10.3389/fnana.2016.00098.
- Hinman, J.R., Brandon, M.P., Climer, J.R., Chapman, G.W., and Hasselmo, M.E. (2016). Multiple Running Speed Signals in Medial Entorhinal Cortex. Neuron 91, 666–679. https://doi.org/10.1016/j.neuron.2016. 06.027.
- Cole, A.E., and Nicoll, R.A. (1984). Characterization of a slow cholinergic post-synaptic potential recorded in vitro from rat hippocampal pyramidal cells. J. Physiol. 352, 173–188. https://doi.org/10.1113/jphysiol.1984. sp015285.
- Dannenberg, H., Young, K., and Hasselmo, M. (2017). Modulation of Hippocampal Circuits by Muscarinic and Nicotinic Receptors. Front. Neural Circuits 11, 102. https://doi.org/10.3389/fncir.2017.00102.
- Wells, C.E., Amos, D.P., Jeewajee, A., Douchamps, V., Rodgers, J., O'Keefe, J., Burgess, N., and Lever, C. (2013). Novelty and Anxiolytic Drugs Dissociate Two Components of Hippocampal Theta in Behaving Rats. J. Neurosci. 33, 8650–8667. https://doi.org/10.1523/JNEUROSCI. 5040-12.2013.
- Muller, R.U., and Kubie, J.L. (1987). The effects of changes in the environment on the spatial firing of hippocampal complex-spike cells. J. Neurosci. 7, 1951–1968. https://doi.org/10.1523/JNEUROSCI.07-07-01951.1987.
- Colgin, L.L., Moser, E.I., and Moser, M.-B. (2008). Understanding memory through hippocampal remapping. Trends Neurosci. 31, 469–477. https:// doi.org/10.1016/j.tins.2008.06.008.

- Palacios-Filardo, J., Udakis, M., Brown, G.A., Tehan, B.G., Congreve, M. S., Nathan, P.J., Brown, A.J.H., and Mellor, J.R. (2021). Acetylcholine prioritises direct synaptic inputs from entorhinal cortex to CA1 by differential modulation of feedforward inhibitory circuits. Nat. Commun. 12, 5475. https://doi.org/10.1038/s41467-021-25280-5.
- Hasselmo, M.E., and Schnell, E. (1994). Laminar selectivity of the cholinergic suppression of synaptic transmission in rat hippocampal region CA1: computational modeling and brain slice physiology. J. Neurosci. 14, 3898–3914. https://doi.org/10.1523/JNEUROSCI.14-06-03898.1994.
- Douchamps, V., Jeewajee, A., Blundell, P., Burgess, N., and Lever, C. (2013). Evidence for Encoding versus Retrieval Scheduling in the Hippocampus by Theta Phase and Acetylcholine. J. Neurosci. 33, 8689–8704. https://doi.org/10.1523/JNEUROSCI.4483-12.2013.
- Sheffield, M.E., and Dombeck, D.A. (2019). Dendritic mechanisms of hippocampal place field formation. Curr. Opin. Neurobiol. 54, 1–11. https:// doi.org/10.1016/j.conb.2018.07.004.
- Bell, L.A., Bell, K.A., and McQuiston, A.R. (2015). Activation of muscarinic receptors by ACh release in hippocampal CA1 depolarizes VIP but has varying effects on parvalbumin-expressing basket cells. J. Physiol. 593, 197–215. https://doi.org/10.1113/jphysiol.2014.277814.
- Schmid, L.C., Mittag, M., Poll, S., Steffen, J., Wagner, J., Geis, H.-R., Schwarz, I., Schmidt, B., Schwarz, M.K., Remy, S., and Fuhrmann, M. (2016). Dysfunction of Somatostatin-Positive Interneurons Associated with Memory Deficits in an Alzheimer's Disease Model. Neuron 92, 114–125. https://doi.org/10.1016/j.neuron.2016.08.034.
- Newman, E.L., Gupta, K., Climer, J.R., Monaghan, C.K., and Hasselmo, M. E. (2012). Cholinergic modulation of cognitive processing: insights drawn from computational models. Front. Behav. Neurosci. 6, 24. https://doi.org/ 10.3389/fnbeh.2012.00024.
- Herrero, J.L., Roberts, M.J., Delicato, L.S., Gieselmann, M.A., Dayan, P., and Thiele, A. (2008). Acetylcholine contributes through muscarinic receptors to attentional modulation in V1. Nature 454, 1110–1114. https://doi.org/10.1038/nature07141.
- Kentros, C.G., Agnihotri, N.T., Streater, S., Hawkins, R.D., and Kandel, E. R. (2004). Increased attention to spatial context increases both place field stability and spatial memory. Neuron 42, 283–295. https://doi.org/10. 1016/s0896-6273(04)00192-8.
- Yu, A.J., and Dayan, P. (2005). Uncertainty, neuromodulation, and attention. Neuron 46, 681–692. https://doi.org/10.1016/j.neuron.2005.04.026.
- Robinson, L., Harbaran, D., and Riedel, G. (2004). Visual acuity in the water maze: sensitivity to muscarinic receptor blockade in rats and mice. Behav. Brain Res. 151, 277–286. https://doi.org/10.1016/j.bbr.2003.09.001.
- Dombeck, D.A., Harvey, C.D., Tian, L., Looger, L.L., and Tank, D.W. (2010). Functional imaging of hippocampal place cells at cellular resolution during virtual navigation. Nat. Neurosci. 13, 1433–1440. https://doi.org/10. 1038/nn.2648.
- Pachitariu, M., Stringer, C., Dipoppa, M., Schröder, S., Rossi, L.F., Dalgleish, H., Carandini, M., and Harris, K.D. (2017). Suite2p: beyond 10,000 neurons with standard two-photon microscopy. Preprint at bioRxiv. https://doi.org/10.1101/061507.
- Climer, J.R., and Dombeck, D.A. (2021). Information Theoretic Approaches to Deciphering the Neural Code with Functional Fluorescence Imaging. eNeuro 8, ENEURO.0266-21.2021. https://doi.org/10.1523/ENEURO.0266-21.2021.
- Harvey, C.D., Collman, F., Dombeck, D.A., and Tank, D.W. (2009). Intracellular dynamics of hippocampal place cells during virtual navigation. Nature 461, 941–946. https://doi.org/10.1038/nature08499.
- Wilson, M.A., and McNaughton, B.L. (1993). Dynamics of the hippocampal ensemble code for space. Science 261, 1055–1058. https://doi.org/10. 1126/science.8351520.
- Mizuseki, K., Royer, S., Diba, K., and Buzsáki, G. (2012). Activity dynamics and behavioral correlates of CA3 and CA1 hippocampal pyramidal neurons. Hippocampus 22, 1659–1680. https://doi.org/10.1002/hipo.22002.





- Danielson, N.B., Zaremba, J.D., Kaifosh, P., Bowler, J., Ladow, M., and Losonczy, A. (2016). Sublayer-specific coding dynamics during spatial navigation and learning in hippocampal area CA1. Neuron 91, 652–665. https://doi.org/10.1016/j.neuron.2016.06.020.
- Pinke, D., Issa, J.B., Dara, G.A., Dobos, G., and Dombeck, D.A. (2023). Full field-of-view virtual reality goggles for mice. Neuron 111, 3941–3952.e6. https://doi.org/10.1016/j.neuron.2023.11.019.
- Zhang, K., Ginzburg, I., McNaughton, B.L., and Sejnowski, T.J. (1998). Interpreting neuronal population activity by reconstruction: unified frame-
- work with application to hippocampal place cells. J. Neurophysiol. 79, 1017–1044. https://doi.org/10.1152/jn.1998.79.2.1017.
- Climer, J.R., Davoudi, H., Oh, J.Y., and Dombeck, D.A. (2025). Hippocampal representations drift in stable multisensory environments. Nature 645, 457–465. https://doi.org/10.1038/s41586-025-09245-y.
- Issa, J.B., Radvansky, B.A., Xuan, F., and Dombeck, D.A. (2024). Lateral entorhinal cortex subpopulations represent experiential epochs surrounding reward. Nat. Neurosci. 27, 536–546. https://doi.org/10.1038/s41593-023-01557-4.



STAR*METHODS

KEY RESOURCES TABLE

REAGENT or RESOURCE	SOURCE	IDENTIFIER	
Bacterial and virus strains			
AAV9-hSyn-GRAB-ACh4l (GRAB-ACh4l also known as GRAB-ACh3.5)	WZ Biosciences	YL001010-AV9	
AAV9-hSyn-GRAB-ACh3.0-mut	WZ Biosciences	YL001004-AV9-PUB	
AA1-CAG-Flex-NES-jRGECO1a-WPRE-SV40	Addgene	100852-AAV1	
AA1-CamKII 0.4-Cre-SV40	Addgene	105558-AAV1	
Experimental models: Organisms/strains			
C57BL/6J mice	Jackson Lab	RRID: IMSR_JAX:000664	
Software and algorithms			
MATLAB	MathWorks	https://www.mathworks.com	
Scanlmage 5.1	MBF Bioscience	https://www.mbfbioscience.com/ products/scanimage	
Clampex 10.3	Moleular Devices	https://www.moleculardevices.com/	
Suite2P	Harris Lab	https://github.com/MouseLand/suite2p	
ViRMEn	Tank Lab	https://github.com/Tank-Lab/ViRMEn	
Deposited data			
Raw and analyzed data, including Imaging and behavioral data	This paper	Available upon request	

EXPERIMENTAL MODEL AND STUDY PARTICIPANT DETAILS

All experiments were approved by the Northwestern University Animal Care and Use Committee. Male C57BL/6J mice (\sim 9 weeks old, The Jackson Laboratory) were used in all experiments. The use of only male mice limits the interpretation of sex on the results found here.

METHOD DETAILS

Mouse surgery

Mice were anesthetized with \sim 1–2% isoflurane. A small (\sim 0.5mm) craniotomy was made over the right dorsal hippocampus at 1.80 mm lateral, 2.30 mm caudal from bregma. For single-color population imaging of ACh release, GRAB-ACh4l (from Yulong Li lab) virus (AAV9-hSyn-GRAB-ACh4l, from WZ Biosciences) was injected using a beveled glass micropipette at the depth of 1250 \pm 10 μ m below dura surface (1 injection of \sim 50nL, 3.3 \times 10 12 GC/mL). For control (mutant) sensor experiments, AAV9-hSyn-GRAB-ACh3.0-mut was used. For dual-color population imaging of ACh release and place cell firing, a mixture of GRAB-ACh4l virus, flexed-jRGECO1a virus (AA1-CAG-Flex-NES-jRGECO1a-WPRE-SV40, 4.0 \times 10 12 GC/mL) and Cre virus (AA1-CamKII 0.4-Cre-SV40, 4.8 \times 10 12 GC/mL) were injected (two injections at 2.20 mm and 2.40 mm caudal from bregma, at 1250 \pm 10 μ m below dura surface, \sim 30nL each site). Mice were subjected to water restriction (0.8–1.0 mL/day) two days after the virus injection surgeries till the end of all experiments. After \sim 5–7 days following water restriction, hippocampal window cannula was implanted as previously described to allow optical access to CA1. The hippocampal window cannula was composed of a 2.77 mm outer diameter and 2.31 mm inner diameter thin-walled stainless steel tube of length 1.5 mm with a 2.5-mm diameter round coverglass sealed to one end. Mice then recovered in the home cage for a week before any training and imaging procedures began.

GRAB-Ach4I

GRAB-ACh4l was engineered from GRAB-ACh3.0 by Yulong Li's lab. GRAB-ACh4l has half maximum effective concentration (EC-50) of $6.6\mu M$ and tau-on of ~ 0.06 sec and tau-off of ~ 0.9 s.

Behavioral training and task in virtual reality

After recovery, mice were trained in the same head-fixed virtual reality system as described previously, ²⁷ consisting of a 5-panel monitor setup, a cylindrical treadmill (read with a rotary encoder) and a water reward delivery spout. Mice traversed in a 3 m virtual





linear track to collect a water reward (4 μ L) at a certain location with 80% reward probability and were teleported back to the beginning of the track after a 3 s delay at the end of the track. A training session usually lasted \sim 45 min for one session per day until the mice reach well-trained criteria, which were (1) mice routinely ran along the track to receive \geq 2 rewards/minute; (2) mice showed anticipatory licking before reward delivery for at least 50% of all trials in a session. Mice usually met the criteria after 4–7 training sessions.

For an environment switching experiment session, well-trained mice first traversed the familiar environment (Fam1) that they were trained in for at least 25 laps, and then the virtual environment was rapidly switched to a novel environment (Nov1) after they were teleported back to the beginning of the Fam1 track. Mice then traversed the Nov1 track for at least 25 laps before the session ended. For the following 3–5 days, mice were placed back into the familiar environment, Fam1, to perform the linear track task. Then the second environment switching session was performed in the exact same way as before, except that mice were switched into a different novel environment (Nov2). Data from the two novel environment switches were grouped together. No differences in the results reported here were observed between the first switch and the second switch as previously reported.

For voluntary disengagement experiments, mice were given $10 \,\mu$ L of water reward (instead of regular $4 \,\mu$ L) for each trial to induce the state of satiation and disengagement within a practical time period (usually 60– $90 \,\mathrm{min}$) in VR. For scopolamine experiments, mice were intraperitoneally injected with saline or scopolamine and allowed to rest $15 \,\mathrm{min}$ in home cages before experiments began. Though the mice used for the voluntary disengagement group were largely the same as the scopolamine group, the imaging datasets were acquired from different fields of view over different days, precluding paired comparisons within each mouse.

Two-photon imaging

A customized Moveable Objective Microscope (Sutter Instruments) with a resonant scanning module (Sutter Instruments) was used for imaging experiments. ^{27,59} A 40x/0.6 NA air objective (LUCPLFLN40×, Olympus) and 40×/0.8 NA water immersion objective (LUCPlanFL N, Olympus) were used for dual-color imaging and multiplane imaging, respectively. Excitation was provided by fixed wavelength Coherent lasers AXON 1064-3 TPC and AXON 920-2 TPC with ~90–130 mW of average power out of the objective. Emission light was split by a 560 longpass dichroic (FF560-Di01, Semrock) and filtered into red (FF01-620/52, Semrock) and green (FF01-510/84, Semrock) channels before being detected by a pair of GaAsP PMTs (H10770PA-40, Hamamatsu Photonics). Imaging was controlled by ScanImage software (Vidrio). A frame sync signal was sent to the data acquisition card (National Instruments) on the VR computer.

For multiplane recordings, an electric lens (EL-10-30-C-VIS-LD, Optotune; f = -100 mm offset lens) was used to switch rapidly between different focal planes. The electric lens was mounted in close proximity to the microscope back aperture and the focal plane was rapidly switched after each collected image of the time-series by changing the applied steady-state current (LD1255R current driver, Thorlabs). Images (512 \times 256 pixels) in each plane were acquired at 10.4 Hz for 3-plane acquisitions. The resulting co-acquired time-series movies contain interleaved frames fast enough to provide sufficient sampling of transients in each plane.

Image processing

For GRAB-ACh4l multi-plane recording, time-series movies were acquired using interleaved frames, such that every third frame corresponded to the same plane during 3-plane imaging. The electric lens settling time of \sim 5 ms between focal planes created distortions in the first few lines of each frame of the movie; these lines were therefore removed before subsequent analysis. Each multiplane time-series was then split into separate time-series movies, one for each acquired plane. Each single-plane time-series was then independently motion corrected using whole frame cross-correlation, as described previously. Our motion correction algorithm uses whole frame cross-correlation and works well so long as there is structure present across the field of view. The GRAB-ACh1 datasets here had significant structure, mostly in the form of blood vessels, but also heterogeneity in indicator expression intensity across the fluorescent neurons (Movies S1 and S2).

For dual-color imaging of GRAB-ACh4l and jRGECO1a, registered (motion correction) of time-series movies and raw fluorescence extraction of putative ROIs were performed using Suite2P, ⁶⁰ with the parameters listing below.

Nplanes	1	nimg_init	300	max_overlap	0.75
nchannels	2	batch_size	500	max_iterations	20
functional_chan	2	smooth_sigma	1.15	high_pass	100
tau	0.6	smooth_sigma_time	0	anatomical_only	0
fs	30.0	maxregshift	0.1	diameter	0
do_bidiphase	0	th_badframes	1	neuropil_extract	1
bidiphase	0	keep_movie_raw	0	allow_overlap	0
multiplane_parallel	0	two_step_registration	0	inner_neuropil_radius	2
ignire_flyback	-1	nonridgid	1	min_neuropil_pixels	350
preclassify	0	block_size	32, 64	soma_crop	1

(Continued on next page)

Article



Continued						
Nplanes	1	nimg_init	300	max_overlap	0.75	
save_mat	1	snr_thresh	1.2	spikedetect	1	
save_NWB	0	maxregshiftNR	5.0	win_baseline	60	
combined	1	1Preg	0	sig_baseline	10	
reg_rig	1	spatial_hp_reg	42.0	neucoeff	0.7	
reg_tif_chan2	1	pre_smooth	0	-	_	
aspect	1	spatial_taper	40.0	-	-	
delete_bin	0	roidetect	1	-	_	
move_bin	0	denoise	1	-	_	
do_registration	1	spatial_scale	0	_	_	
align_by_chan	2	threshold_scaling	2.0	-	-	

GRAB-ACh signal analysis

After motion correction, time-series movies of GRAB-ACh4l fluorescence were analyzed in two main ways. For spatial heterogeneity analysis (Figure 1), each imaging field was divided into a grid of smaller subregions (ROIs) at different resolutions (4×4 , 12×12 , 60×60 , and 124×124), and average $\Delta F/F$ signals were computed for each subregion. Prior to analysis, dim pixels were excluded by thresholding: only pixels with intensity above the 30th percentile of the whole-field intensity distribution were retained. For each grid size, an ROI was included in subsequent distance vs. correlation analyses only if it contained a sufficient proportion of non-dim pixels—specifically, >50% for 4×4 and 12×12 grids, >75% for 60×60 , and 100% for 124×124 .

For population-level signal dynamics (Figures 2, 3, 4, 5), whole-frame average GRAB-ACh4l signals were computed from each frame of the time-series movie. For Figures 2 and 3, Δ F/F traces were generated using the median fluorescence across the entire session as the baseline (F_0). For Figures 4 and 5, Δ F/F traces were computed separately for each condition (e.g., engaged vs. disengaged, saline vs. high/low scopolamine), with F_0 defined as the median fluorescence value for each condition-specific trace. This was done to account for any slow changes in baseline that could occur across the long time experiments across conditions. To avoid introducing artifacts, no additional fitting or baseline correction algorithms were applied. The same image processing, intensity thresholding, and signal extraction procedures were applied to the control sensor datasets (e.g., GRAB-ACh mut) to allow for direct comparisons across conditions.

Deconvolution of GRAB-ACh signals

To estimate the underlying acetylcholine (ACh) release dynamics from GRAB-ACh4l fluorescence signals (from *in vivo* measurements), we performed Wiener deconvolution using a bi-exponential impulse response model that accounts for both the sensor's rise and decay kinetics. The impulse response kernel was defined as

$$k(t) = \frac{1}{\tau_{off} - \tau_{on}} \left(e^{-t_{/\tau_{off}}} - e^{-t_{/\tau_{on}}} \right)$$

Where τ_{on} and τ_{off} are the rise and decay time constants of the sensor, respectively. The kernel was normalized to unit area under its curve and used in the frequency domain to perform Wiener deconvolution. Specifically, the deconvolved signal $\widehat{X}(f)$ was computed as:

$$\widehat{X}(f) = \frac{Y(f) \cdot H * (f)}{|H(f)|^2 + \lambda^2}$$

where Y(f) and H(f) are the Fourier transforms of the raw fluorescence signal and the kernel, respectively, $H^*(f)$ is the complex conjugate of H(f), and λ is a regularization parameter that was optimized by minimizing the reconstruction error between the raw and re-convolved signal. The final deconvolved trace was smoothed using a Gaussian filter (100 ms window) to reduce high-frequency noise. GRAB-ACh4l fluorescence vs. time traces were deconvolved using a bi-exponential kernel with time constants $\tau_{\text{on}} = 0.06$ s and $\tau_{\text{off}} = 1$ s; these deconvolved traces were used for all figures and analysis after Figure 1.

GLM analysis

To model the contributions of behavior to acetylcholine (ACh) dynamics, we used a ridge-regularized generalized linear model (GLM) applied to deconvolved GRAB-ACh Δ F/F signals. Prior to modeling, raw fluorescence signals were deconvolved using a bi-exponential kernel with time constants $\tau_{on} = 0.06$ s and $\tau_{off} = 1$ s to approximate the underlying ACh concentration dynamics.

The design matrix of predictors was constructed as follows.





- (1) Continuous running speed was included as both a linear and quadratic term to account for potential nonlinear modulation of ACh by speed.
- (2) Binary speed was calculated as a thresholded version of running speed (1 if speed >0.5 cm/s, otherwise 0) to capture engagement in locomotion vs. immobility.
- (3) Reward timing was included by appending a series of lagged binary impulse vectors (from 0 to 2 s in 100 ms steps), representing recent reward delivery history.
- (4) Licking behavior was similarly represented by time-lagged lick vectors over the same 2-s (100 ms step) window

All predictors were z-scored before model fitting. We used a 10-fold cross-validation procedure to evaluate performance and selected the optimal ridge penalty λ from a logarithmically spaced grid $(10^{-2} \text{ to } 10^2)$ based on mean squared error. For each session, we computed the total explained variance (R²), and also calculated the variance explained by each predictor group by projecting the model weights onto the corresponding columns of the design matrix (i.e., speed, binary speed, reward history, and lick history).

This modeling framework was applied to three experimental contexts.

- (1) In the familiar environment, the model captured substantial trial-by-trial variance in ACh with speed being the dominant predictor (Figure 2).
- (2) To test whether novelty-induced ACh increases could be explained by behavioral changes, we trained the model on the familiar environment data before a VR environment switch and tested it on the novel environment data (Figure S4).
- (3) In the engaged vs. disengaged analysis, we trained the model on the engaged periods and tested it on the disengaged periods, using the same procedure as for the novel vs. familiar environment analysis (Figure S5).

Place cell identification and analysis

Extracted calcium fluorescence traces were exported from suite2P and imported into MATLAB for identifying significant calcium transients as described previously.⁵⁹ Briefly, slow time-course changes in the fluorescence traces were removed by calculating the distribution of fluorescence in a 20s time window around each time point and subtracting the 8th percentile value of the distribution. The baseline subtracted traces were then subjected to the analysis of the ratio of positive-to negative-going transients of various amplitudes and durations. This resulted in the identification of significant transients with less than 1% false positive rate. The significant transients were left untouched while all other values in the trace were set to 0. The resulting traces of all ROIs were used for further data analysis.

Fluorescence tuning maps were made by binning the position across the track into 60 bins (bin width = 0.05 m) and identifying the mean fluorescence where the mouse was moving at least 0.1 cm/s. To test if a cell is a place cell, we computed the spatial information I in bits per action potential for the fluorescence tuning map⁶¹:

$$I = \frac{1}{f} \sum_{i=1}^{N} f_i P_X(x_i) \log_2 \left(\frac{f_i}{f}\right)$$

Where f is the mean fluorescence of the neuron across all time points of navigation, i is the spatial bin number, N is the total number of spatial bins, f_i is the mean fluorescence of the neuron in spatial bin i, and $P_X(x_i)$ is the probability of the mouse occupying spatial bin i.

To build a null distribution of information *I* for each neuron, we shuffled the fluorescence trace with regard to position and recalculated the tuning map 1000 times. A cell was a significant place cell if it had higher information than 99% of these shuffle epochs and had an information of at least 0.5 bits per action potential.

For the analysis of the percentage of place cells, the same number of frames of the recorded movies among conditions (engaged vs. disengaged, saline vs. high/low scopolamine) were used to identify place cells. The percentage of place cells varies widely across studies, and our percentages are within the range from prior research.^{29,59,62–66} Place cell reliability was defined as the Pearson correlation between the activity on each trial to the mean activity of the whole session.

Behavior analysis

Sessions were divided into engaged vs. disengaged periods based on behavioral criteria.

- (1) Engaged: Speed reduction >50% in reward zone vs. track average, average of >2 anticipatory licks in 1s window before
- (2) Disengaged: Speed reduction <25% in reward zone, average of <1 anticipatory licks before reward.
- (3) Sessions not meeting either criterion were excluded from disengaged state analysis.

Bayesian decoding

To quantify the accuracy of population coding of CA1 neurons under different experimental conditions (voluntary disengagement or scopolamine administration), we used Bayesian reconstruction based on a method described previously.⁶⁷ Decoding was performed



on the likelihood that a significant transient occurred in a time frame during navigation, trained on all trials of the session except one, and tested on the one trial that was left out. This process was repeated to test each trial. The session was divided into time bins of $\Delta t = 0.1$ s. For each time bin n, the conditional likelihood that the mouse was in position bin x_i (bin width = 0.10 m) given the number of time points with significant transients in that bin was:

$$p(x_i|n) = p_X(x_i) \left(\prod_{i=1}^M f_{ij} \right) e^{-k \sum_{i=1}^M \lambda_{ij}}$$

Where $p_X(x_i)$ is the probability that the mouse is in the *i*th spatial bin during a time sample, f_{ij} is the average rate of time points with significant transients by the *j*th neuron in the *i*th spatial bin during a time sample, n_j is the number of time points with significant transients observed during the time window in neuron *j*, and M is the total number of neurons. The decoded position was selected as the one with maximum conditional likelihood. For the analysis of decoding error, the same number of frames of the recorded movies among conditions (engaged vs. disengaged, saline vs. high/low scopolamine) were used.

QUANTIFICATION AND STATISTICAL ANALYSIS

All data were analyzed using custom MATLAB scripts. Sample sizes were not predetermined statistically, and the experimenter was aware of the experimental conditions. Non-parametric and parametric statistical tests were used as indicated in the text and figure legends (Kruskal-Wallis test with post-hoc pairwise comparisons and Wilcoxon signed-rank test). Exact p values are listed and *, *** in the figures refer to p < 0.05, p < 0.01 respectively; n.s. not significant.